Archiv der Pharmazie

DPhG

FULL PAPER

Revealing a Gold Mine of Bioactive Compounds From Natural Sources Using In Vitro, In Silico, and Network Pharmacology: A Case Study on *Cachrys cristata*

Inci Kurt-Celep[1] | Shakeel Ahmed[2] | Mehmet Veysi Cetiz[3] | Abdullahi Ibrahim Uba[4] | Gunes Ak[2] | Selami Selvi[5] | Ahmet Emir[6] | Stefano Dall'Acqua[7] | Gokhan Zengin[2]

[1]Department of Biotechnology, Faculty of Pharmacy, İstanbul Okan University, Tuzla, Istanbul, Turkey | [2]Department of Biology, Science Faculty, Selcuk University, Konya, Turkey | [3]Department of Medical Biochemistry, Faculty of Medicine, Harran University, Sanliurfa, Turkey | [4]Department of Molecular Biology and Genetics, Istanbul AREL University, Istanbul, Turkey | [5]Department of Plant and Animal Production, Altınoluk Vocational School, Balıkesir University, Balıkesir, Turkiye | [6]Department of Pharmacognosy, Faculty of Pharmacy, Ege University, Bornova, Izmir, Turkey | [7]Department of Pharmaceutical and Pharmacological Sciences, University of Padova, Padua, Italy

Correspondence: Gokhan Zengin (gokhanzengin@selcuk.edu.tr)

Received: 17 April 2025 | **Revised:** 25 June 2025 | **Accepted:** 29 June 2025

Funding: The authors received no specific funding for this work.

Keywords: *Cachrys* cristata | enzyme inhibition | network pharmacology | radical scavenging | UV-induced skin damage

ABSTRACT

The study aimed to explore the chemical composition and assess the wide-ranging biological effects of *Cachrys cristata* extracts, including ethyl acetate, ethanol, ethanol/water (70%), and water. We evaluated the bioactive potential of these extracts by different chemical techniques such as radical scavenging, reducing power, and metal chelation assays. Additionally, we conducted enzyme inhibition assays to target cholinesterase, tyrosinase, amylase, glucosidase, elastase, collagenase, and hyaluronidase. In the profile analysis, we determined that the main components are phenolic acids, mainly caffeic acid with the highest concentrations. The water extract of the plant showed the highest concentration of phytochemicals and superior antioxidant activity. In addition, the ethanol and ethyl acetate extracts showed the greatest level of inhibition of most of the evaluated enzymes. On the other hand, its potential protective effects against UV-induced oxidative stress, genotoxicity, and extracellular matrix (ECM) degradation were investigated. Different extracts of the plant were evaluated in terms of their effects on DNA damage, cellular viability, ECM enzymes, and matrix metalloproteinases (MMPs). COMET analysis showed that DNA breaks and genotoxicity caused by UV rays were significantly suppressed, especially by the water extract. Furthermore, network pharmacology analyses, in conjunction with in silico molecular docking and molecular dynamics simulations, demonstrated robust ligand–protein interactions and furnished insights into the underlying mechanisms, thereby substantiating the plant's therapeutic potential. Overall, our research highlights the significant potential of *C. cristata* as a valuable reservoir of bioactive chemicals that can be utilized in the health and wellness industries.

1 | Introduction

During oxidative metabolism in aerobic organisms, reactive oxygen species (ROS) are generated. Under typical circumstances, the production and removal of ROS are in a stable equilibrium. Nevertheless, when faced with internal or external environmental challenges like elevated glucose levels or UV radiation, there can be a substantial rise in ROS generation, resulting in oxidative stress. Excessive ROS production can harm biomolecules and is linked to the development of various diseases like diabetes, metabolic syndrome, skin conditions, tumors, Alzheimer's and Parkinson's

diseases, autoimmune disorders, male and female infertility, and more [1, 2].

Traditional medicine has relied on plants as a vital source of bioceuticals for treating and preventing several ailments across generations [3, 4]. Despite significant advancements in modern medicine, a large portion of the global population, especially those with poor incomes, still rely on traditional therapy methods using natural products to cure various illnesses [5, 6]. The widespread usage of these therapy approaches is mostly based on old wisdom, local belief, efficacy, and affordability [7]. The current rise of pandemics has sparked fresh interest in utilizing natural resources, such as plant-based materials and their components, like nutraceuticals [8]. Plant materials are typically dried, pulverized, or extracted to create compounds known as herbal or botanical medicines [9, 10]. Commercial medications have been developed from plant sources, which provide various advantages in discovering new pharmaceuticals due to their widespread availability in nature and diverse geographic distribution [11, 12]. Modern medications primarily utilize single ingredients to maintain consistent efficacy and purity, in contrast to the use of extracts [13]. However, contemporary drug development techniques continue to heavily rely on extracting compounds from natural sources, altering existing phytotherapeutics, and creating synthetic molecules that imitate natural ingredients [14].

The *Cachrys* L. genus is part of the Apiaceae family and has a broad distribution in the Mediterranean basin, with plant species that are unique to southern Europe, Asia, and northern Africa. The species from this genus can be found in various countries, including Turkey, Serbia, Bulgaria, Albania, Iran, Greece, Algeria, Italy, Spain, Libya, Tunisia, and some others [15]. It consists of about 15 known and 11 accepted species including *C. cristata* [16]. Several studies have investigated the phytochemical profile of different plant species of *Cachrys* spp. and their potential impact on human ailments. The studies primarily concentrated on the essential oils extracted from these plants, highlighting that *Cachrys* species are abundant in coumarins, particularly furanocoumarins. Additional plant compounds, like flavonoids (hesperidin, naringin, and quercitrin), terpenes (limonene, anethole, estragole, etc.), coumarins (bergapten, seselin, osthol, etc.), phytosterols, and fatty acids (myristic, palmitic, α-linolenic acid, etc.) are also present [17–20]. Furthermore, several biological properties have been evaluated, including antioxidant, antimicrobial, anti-inflammatory, cytotoxic effects, and inhibition of different enzymes [19, 21]. These species have been employed in Turkish traditional medicine as a tonic to treat intestinal worms [18, 22].

C. cristata DC., also known as English spiny basil or Serb. krestasti kahris is a perennial plant [23]. In Turkey, it is commonly used as a condiment in various food products and is traditionally included in tarhana soup [24]. Considering the paucity of research on *C. cristata*, we decided to utilize it in our current research. We used HPLC-MS to perform comprehensive chemical characterization and quantification of the different extracts obtained from the extraction of the aerial parts of the plant. Furthermore, we evaluated enzyme inhibition for the first time and investigated its antioxidant potential using five different techniques. This study also aimed to elucidate the chemical composition and wide-ranging biological properties of *C. cristata* extracts, with a particular focus on their cytoprotective potential and biological safety. To this end, in vitro cellular assays were conducted using human dermal fibroblast (HDF) cells. Cytotoxicity and cell viability were assessed via WST-1 assay across a range of concentrations (25–200 μg/mL), while UV-induced oxidative stress and DNA damage models were evaluated using DCFDA and COMET assays, respectively. These analyses were designed to determine whether phytochemical constituents confer protective effects under oxidative stress conditions. To further elucidate the potential therapeutic effects of *C. cristata*, integrative computational strategies have been employed. Network pharmacology analyses provide a systems-level perspective on the molecular targets and pathways influenced by the plant's phytochemicals, while in silico molecular docking facilitates the prediction of the binding affinities and orientations of these compounds to their respective protein targets. Furthermore, molecular dynamics (MD) simulations provide insights into the stability and conformational dynamics of ligand–protein complexes over time, thus contributing to a deeper understanding of their potential biological activities and mechanisms of action.

2 | Results and Discussion

2.1 | Total Phenolic and Flavonoid Contents

Polyphenols are bioactive compounds derived from plants that have been significant in disease prevention. Phenolics and flavonoids are essential phytochemicals and have redox characteristics that initiate antioxidant activity. The hydroxyl groups present in polyphenols enable the scavenging of free radicals [25, 26]. The total phenolic contents of the plant extracts analyzed are presented in Table 1, determined as gallic acid (GA) equivalents per gram of dry extract, varied from 19.30 to 30.15 mg GA/g dry extract. The plant's ethanol extract showed the highest phenolic contents, while ethanol/water (70%) provided the minimum contents.

The levels of flavonoids in plant extracts varied from 9.13 to 4.56 mg RE/g dry extract. The ethanol extract of the aerial parts

TABLE 1 | Extraction yields (%) and total phenolic and flavonoid contents in the tested extracts.

Extracts	Extraction yields (%)	TPC (mg GAE/g dry extract)	TFC (mg RE/g dry extract)
Ethyl acetate	5.98	29.36 ± 0.60^{b}	5.52 ± 0.09^{b}
Ethanol	11.05	30.15 ± 0.22^{a}	9.13 ± 0.18^{a}
Ethanol/Water (70%)	10.99	19.39 ± 0.17^{c}	4.58 ± 0.08^{c}
Water (infused)	13.21	28.40 ± 0.35^{b}	4.65 ± 0.40^{c}

Note: Values are reported as mean ± SD of three parallel measurements. Different letters indicate significant differences among the tested extracts ($p < 0.05$).
Abbreviations: GAE, gallic acid equivalents; RE, rutin equivalents.

showed the highest flavonoid contents, while water the minimum levels. Flavonoids play a crucial role in both human and animal diets due to their abundance in plants. The results demonstrated that the solvents utilized for extraction are accountable for dissolving both groups of compounds in plants. In a previous study, Matejic et al. [27] also demonstrated the presence of total phenolic and flavonoid contents in the different extracts of *C. cristata*. Although they used more organic solvents for the extraction of extracts, they had a variability with some of our results.

2.2 | Chemical Identification

Table 2 displays the quantification of different identified compounds present in five different extracts of *C. cristata* using a variety of extraction solvents. All the compounds presented in the table were quantified in milligrams per kilogram (μg/g dry extract). Phenolic acids, including syringic acid and vanillic acid, were identified in the samples obtained from diverse sources. Syringic acid was detected in water extracts (WEs) in minute quantities, whereas vanillic acid displayed moderate concentrations in all solvent combinations, with particular emphasis on ethanol/water and ethanol extracts. The presence of substantial quantities of carboxylic acid (benzoic acid) in ethanol/water and WEs suggests that the compound is soluble in aqueous solutions. On the other hand, significant concentrations of hydroxybenzoic acids, such as 4-hydroxybenzoic acid, were observed in all solvents. Notably, WEs contained the maximum levels of these acids, indicating that they are soluble in polar solvents. Ferulic acid, which is classified as a phenolic acid, demonstrated moderate concentrations in all solvents, although WEs contained marginally higher levels. In a similar vein, chlorogenic acid, which is classified as a phenolic acid as well, was found in considerable amounts in extracts of water and ethanol.

Caffeic acid, which is a member of the phenolic acid class, exhibited the most significant concentrations among the compounds that were examined, particularly in the WEs. P-coumaric acid, an additional phenolic acid, was found in significant concentrations in all solvents, albeit marginally higher in ethanol and ethanol/WEs than in ethyl acetate.

TABLE 2 | Chemical composition of the tested extracts (μg/g dry extract).

Compound name	Molecular formula	Exact mass	Ethyl acetate	Ethanol	Ethanol/Water	Water
Syringic acid	$C_9H_{10}O_5$	197.45	nd	nd	nd	14.06 ± 1.22
Vanillic acid	C_8H_8O4	167.0344	61.23 ± 2.13	79.73 ± 0.48	134.92 ± 0.23	140.05 ± 0.78
Benzoic acid	$C_7H_6O_2$	121.0289	nd	nd	621.59 ± 1.42	554.57 ± 1.61
4-Hydroxybenzoic acid	$C_7H_6O_3$	137.0239	25.89 ± 0.97	67.54 ± 0.97	176.46 ± 0.89	345.38 ± 1.58
3-Hydroxybenzoic acid	$C_7H_6O_3$	137.0239	nd	nd	nd	nd
Ferulic acid	$C_{10}H_{10}O_4$	193.0501	9.83 ± 1.48	15.71 ± 3.66	13.65 ± 3.16	21.12 ± 3.09
Chlorogenic acid	$C_{16}H_{18}O_9$	353.0872	39.56 ± 0.38	397.83 ± 1.45	87.99 ± 2.53	345.16 ± 1.27
Caffeic acid	$C_9H_8O_4$	179.5959	4366.79 ± 3.06	6868.55 ± 0.28	3377.49 ± 2.28	22373.65 ± 4.02
p-Coumaric acid	$C_9H_8O_3$	163.0395	35.46 ± 4.17	126.49 ± 3.77	102.18 ± 1.79	104.46 ± 1.13
Hesperidin	$C_{28}H_{34}O_{15}$	609.1819	34.56 ± 1.55	531.92 ± 2.08	468.95 ± 1.43	184.76 ± 0.99
Rutin	$C_{27}H_{30}O_{16}$	609.1456	280.94 ± 0.72	3931.10 ± 2.39	3556.04 ± 0.82	1402.24 ± 2.31
Fisetin	$C_{15}H_{10}O_6$	285.0399	62.09 ± 3.08	27.20 ± 0.83	8.15 ± 2.49	8.27 ± 1.44
Morin	$C_{15}H_{10}O_7$	301.0348	87.63 ± 2.91	nd	nd	99.78 ± 2.71
Quercetin	$C_{15}H_{10}O_7$	301.0348	366.13 ± 1.22	68.62 ± 1.39	46.23 ± 1.77	1586.50 ± 2.56
Daidzein	$C_{15}H_{10}O_4$	253.0501	1.25 ± 3.64	1.68 ± 0.98	1.33 ± 1.02	0.82 ± 1.39
Isorhamnetin	$C_{16}H_{12}O_7$	315.0505	nd	nd	3.65 ± 0.88	nd
Naringenin	$C_{15}H_{12}O_5$	271.0606	154.88 ± 1.08	168.02 ± 1.71	51.23 ± 2.04	19.02 ± 0.55
Luteolin	$C_{15}H_{10}O_6$	285.0399	123.39 ± 1.75	42.38 ± 2.88	21.05 ± 1.32	13.40 ± 1.81
Galangin	$C_{15}H_{10}O_5$	269.045	56.41 ± 1.58	12.40 ± 1.31	8.29 ± 3.48	4.76 ± 3.19
Kaempferol	$C_{15}H_{10}O_6$	285.0399	13.70 ± 4.16	4.27 ± 0.69	2.01 ± 2.33	1.96 ± 1.43
Chrysin	$C_{15}H_{10}O_4$	253.0501	9.02 ± 0.79	3.07 ± 2.19	1.61 ± 1.26	1.24 ± 0.39
Vitexin	$C_{21}H_{20}O_{10}$	431.0978	0.55 ± 1.30	6.77 ± 1.28	20.55 ± 2.77	3.25 ± 1.62
Genistein	$C_{15}H_{10}O_5$	269.045	4.90 ± 2.23	1.84 ± 0.72	nd	0.87 ± 1.53
Apigenin	$C_{15}H_{10}O_5$	269.045	12.72 ± 4.16	2.61 ± 0.98	191.93 ± 0.94	1.65 ± 0.75
Syringin	$C_{17}H_{24}O_9$	371.1342	853.90 ± 3.44	nd	4834.53 ± 3.65	3404.75 ± 4.07
Catechol	$C_6H_6O_2$	109.0289	1003.54 ± 1.73	3512.99 ± 1.59	18842.52 ± 3.07	16968.02 ± 1.99

Abbreviation: nd, no detected.

The ethanol and ethanol/WEs contained moderate to significant concentrations of flavonoid glycosides, including rutin, which was especially abundant in both solvents. The flavonols fisetin and morin demonstrated moderate levels of concentration in all solvents, although ethyl acetate and WEs contained marginally higher concentrations of fisetin. Another flavonol, quercetin, was detectable in considerable amounts across all solvents, with particular emphasis on WEs. Naringenin and other flavanones demonstrated significant concentrations in various solvents, with ethanol and ethyl acetate extracts containing the maximum levels. Flavonoids such as galangin and luteolin were detected in moderate concentrations in all solvents, with ethyl acetate exhibiting marginally higher levels. Furthermore, the flavone compounds apigenin and chrysin were observed in moderate concentrations, with chrysin exhibiting marginally elevated levels in ethyl acetate.

Trace quantities of flavone C-glycosides, such as vitexin, were detected in ethyl acetate and WEs, whereas the ethanol/WEs contained moderate concentrations. Trace quantities of isoflavones, such as genistein and daidzein, were detected in all solvents, suggesting that their presence in the samples was minimal. Phenolic glycosides, including syringin, demonstrated notable concentrations in ethanol/water and WEs, which indicates that they are exceptionally soluble in aqueous solutions. In conclusion, substantial concentrations of catechol, a phenolic compound, were detected in all of the extracts, particularly in the ethanol/water and WEs, suggesting that it was abundant in the samples. The results of this study underscore the wide range of substances that are found in the extracts, exhibiting variations in concentrations and solubilities when tested in distinct solvents.

A previous work focused on analyzing the ethyl acetate fraction obtained from the aerial portions of *C. pungens* using high-performance thin-layer chromatography (HPTLC) in a methanolic extract. They detected many substances that are present in our identified list of chemicals, confirming their presence in the plant of *Cachrys* species. These compounds include catechin, flavonoid glycosides such as naringin and quercitrin, cinnamic acids such as caffeic and ferulic acids, as well as GA, a phenolic acid [28].

2.3 | Antioxidant Activities

Antioxidant molecules hinder the oxidation of substrates, and their impacts are assessed by several methods. Lack of strong antioxidant activity in an extract does not necessarily mean low quality, as extracts contain different chemical components with unique responses [29]. The importance of plants in evaluation is indicated by the existence of total phenolics and flavonoids [30], since diverse experimental circumstances and assay principles are utilized in various ways to measure antioxidant activity.

To our knowledge, very few studies are present for the evaluation of the antioxidant potential of *C. cristata* with a limited number of assays like DPPH and ABTS. In our study, we assess the antioxidant activity using six different spectrophotometric methods: DPPH, FRAP, ABTS, CUPRAC, PBD, and MCA assays. Among the tested extracts, WE exhibited highest antioxidant activity in the following order in various antioxidant assays (Table 2): CUPRAC (56.81 mg TE/g dry extract), ABTS (53.82 mg TE/g dry extract), FRAP (32.97 mg TE/g dry extract), MCA (26.39 mg EDTAE/g dry extract), and DPPH (20.15 mg TE/g dry extract), while lowest activity was obtained with PBD assay (0.79 TE/g dry extract). Ethyle acetate extracts displayed the minimum antioxidant potential as compared with the other extracts obtained by different solvents using the same methods, but interestingly, it provide the high values for antioxidant potential with MCA (21.93 EDTAE/g dry extract) and PBD (1.21 TE/g dry extract) assays as compared with others. This difference in the activities by the evaluated assays is likely linked to the chemical composition of the extract, containing specific chemicals with a higher affinity for radical inhibition and reduction compared with those involved in the main mechanism in PBD and MCA testing. This experimental outcome aligned with prior results, indicating water as the most active extract among others. Matejic et al. used the DPPH and ABTS assays to examine the antioxidant characteristics of extracts from the above-ground parts and fruits of *C. cristata*. With an IC_{50} value of 1.784 mg/mL, the fruit WE exhibited the strongest radical scavenging activity. IC_{50} values of 3.347 and 4.058 mg/mL were obtained from the methanolic extracts of the fruits and aerial parts, respectively. With a measurement of 3 mg of vitamin C per milliliter of extract, the acetone extract from the upper sections of *C. cristata* demonstrated the highest antioxidant capacity in the ABTS assay [27].

The antioxidant activity of the extracts can be correlated to the existence and level of constituents of the specific extract. The antioxidant activity of water and ethanol/WEs is principally attributed to their abundant concentration of flavonoids and phenolic chemicals, which are widely recognized for their strong antioxidant capabilities [31–33]. The extracts contain substantial quantities of caffeic acid, chlorogenic acid, quercetin, rutin, fisetin, morin, naringenin, luteolin, galangin, kaempferol, chrysin, apigenin, and catechol. The chemicals listed above demonstrate various antioxidant capabilities, such as the capability to chelate metal ions and remove free radicals. These combined effects boost the antioxidant capacity of the extracts. The improved solubility of these antioxidant chemicals in ethanol/water solvents and water makes it easier to extract them, resulting in higher concentrations and, as a result, increased antioxidant activity was observed in the results. Although the antioxidant activity of the ethanol extract is significantly lower than that of the water and ethanol/WEs, it nevertheless exhibits substantial potential as an antioxidant. The presence of chemicals such as vitexin, vanillic acid, and ferulic acid relates to this, but they are found in slightly lower concentrations. On the other hand, the ethyl acetate extract has a lower amount of antioxidant components, such as daidzein and p-coumaric acid, which leads to a comparatively lower level of antioxidant activity. The polarity of water and ethanol solvents facilitates the extraction of various antioxidant chemicals from the sample matrix, resulting in extracts that have increased antioxidant activity. The choice of solvent considerably affects the antioxidant capacity of the extracts [34]. The water and ethanol/WEs demonstrate the highest antioxidant activity since they have the capacity to extract a significant amount of antioxidant-rich chemicals from the sample's matrix.

2.4 | Enzyme Inhibition Activities

Contemporary research is increasingly focusing on natural sources of bioactive chemicals in the search for new therapeutic treatments, as these molecules are effective and have few adverse effects. Recent research indicates that specific plant-based substances have the capacity to control or suppress the excessive activity of enzymes linked to the advancement of diseases, including neurodegenerative diseases, diabetes, and other metabolic disorders [35].

To explore the enzyme inhibitory capabilities of the different extracts of *C. cristata*, a number of enzymes were tested. These enzymes included acetylcholinesterase (AChE), butyrylcholinesterase (BChE), α-amylase, α-glucosidase, and tyrosinase. The results are summarized in Table 3.

The AChE inhibitory ability of ethanol extract was found to be the greatest, with 3.55 mg GALAE/g dry extract. This was followed by ethanol/water (70%) extract, which had 3.32 mg GALAE/g dry extract, and ethyl acetate extract, which had 3.14 mg GALAE/g dry extract. The AChE inhibition assay yielded the lowest activity for water infusion. It is possible to arrange the BChE inhibition ability in the following order: water > ethanol > ethanol/water (70%) > ethyl acetate. Surprisingly, the water gives the highest values for BChE (3.86 mg GALAE/g dry extract), which was the lowest one for the inhibition of AChE.

The principal enzyme AChE is accountable for the hydrolysis of acetylcholine. The treatment approach for Alzheimer's disease (AD), along with other neurological disorders including senile dementia, myasthenia gravis, and ataxia, centers around the inhibition of this enzyme [36, 37]. While BChE exerts a restricted influence on acetylcholine homeostasis in the brain [38], its activity is elevated in AD patients [39]. There is no previous study available on the inhibition of these two important enzymes by *C. cristata* and here is the first time we investigated the potential of this plant against these important enzymes associated with neurodegenerative disorders. The results correspond to the available data for the other plant species of the genus that demonstrated noteworthy inhibitory impacts on these enzymes. The inhibitory effects of *C. sicula* on the AChE and BChE enzymes were evaluated by Tahar et al. By hydrodistilling the essential oil from the leaf of the plant, its biological activity was evaluated in the presence of butyrylthiocholine chloride and acetylthiocholine iodide as reaction substrates. Significant inhibition of BChE was observed with an IC_{50} value of 91.90 ± 0.00 μg/mL for the essential oil derived from *C. sicula*. Mild inhibition of AChE was demonstrated with an IC_{50} of 169.91 ± 0.00 μg/mL [40]. The anti-tyrosinase activity of the MeOH extract of *Prangos heyniae* H. was quantified by an IC_{50} value of 543.37 ± 7.45 μg/mL. The inhibitory activities of AChE and BChE were observed in the CHCl3 extract, with IC_{50} values of 273.92 ± 32.07 and 38.68 ± 2.56 μg/mL, respectively [41]. In another study of the same family species, Nilofar et al. demonstrated the inhibitory effects of AChE and BChE in *Hippomarathrum scabrum* extracts from turkey [42]. The data provide confirmation of the activity of the same family plants as potential cholinesterase inhibitors and need more detailed study for further associated mechanisms.

On the other hand, it was demonstrated that ethanol/water (70%) and ethanol-alone extracts exhibited the most robust capacity to inhibit tyrosinase (41.26 mg KAE/g dry extract and 40.06 mg KAE/g dry extract, respectively). Conversely, the tyrosinase inhibitory effect observed in water (infused) was comparatively very weak (9.66 mg KAE/g) than the inhibition of cholinesterase. Tyrosinase, a pivotal enzyme in the production of melanin, plays a vital role in preserving the skin's defense against harmful UV radiation. Excessive production of melanin can lead to pigmentation problems, such as the development of dark patches or premature aging spots. To prevent excessive melanin formation and its effects on skin pigmentation, it is crucial to regulate the activity of tyrosinase.

Efforts to effectively control chronic hyperglycemia involve a continuous focus on exploring and developing inhibitors that target important pharmacological targets, such as α-glucosidase and α-amylase [43]. This technique shows great potential for tackling this illness and is one of the main focuses of our ongoing research effort to explore the new natural inhibitors from the plant sources.

According to our findings, at different concentrations, the amylase inhibition capacities varied between 0.65 mmol and 0.05 mmol ACAE/g of dry plant extracts in the following order: ethyl acetate water > ethanol > ethanol/water (70%) > water. The activity of glucosidase was impeded only by ethanol/water (70%) extract (1.45 mmol ACAE/g dry extract) and water (0.05 mmol ACAE/g dry extract), while ethyl acetate and

TABLE 3 | Antioxidant properties of the tested extracts.

Extracts	DPPH (mg TE/g dry extract)	ABTS (mg TE/g dry extract)	CUPRAC (mg TE/g dry extract)	FRAP (mg TE/g dry extract)	Chelating (mg EDTAE/g dry extract)	PBD (mmol TE/g dry extract)
Ethyl acetate	1.95 ± 0.36^{d}	25.18 ± 0.07^{c}	35.17 ± 0.67^{d}	23.06 ± 0.25^{c}	21.83 ± 0.16^{b}	1.21 ± 0.06^{a}
Ethanol	8.15 ± 0.55^{b}	31.37 ± 0.34^{b}	52.53 ± 2.16^{b}	28.55 ± 0.32^{b}	8.20 ± 0.71^{d}	1.29 ± 0.02^{a}
Ethanol/water (70%)	7.73 ± 0.14^{c}	34.97 ± 0.61^{b}	40.72 ± 0.68^{c}	22.12 ± 0.10^{d}	11.59 ± 0.70^{c}	0.72 ± 0.03^{c}
Water (infused)	20.15 ± 0.29^{a}	53.82 ± 0.72^{a}	56.81 ± 0.41^{a}	32.97 ± 1.09^{a}	26.39 ± 0.07^{a}	0.79 ± 0.04^{b}

Note: Values are reported as mean ± SD of three parallel measurements. Different letters indicate significant differences among the tested extracts ($p < 0.05$).
Abbreviations: EDTAE, EDTA equivalent; MCA, metal chelating activity; PBD, phosphomolybdenum; TE, trolox equivalent.

ethanol did not show any kind of activity (Table 4). Regarding glucosidase inhibition specifically, ethanol and ethyl acetate extracts may not demonstrate significant activity, while other solvents manifest some inhibitory effects. This variation might stem from the presence of specific compounds like hesperidin, rutin, quercetin, fisetin, naringenin, kaempferol, and vitexin in water and ethanol/WEs, known for their glucosidase inhibitory properties [44–46]. Their absence or lower concentration in ethanol and ethyl acetate extracts could explain the observed lack of glucosidase inhibition in these solvents.

The enzyme-inhibitory effects of extracts obtained from members of the *Cachrys* species, to the best of our knowledge, have been the topic of a limited amount of research. A further point to consider is that there is currently no information available concerning the inhibitory effects of *C. cristata* except a few studies on its antioxidant activity [27]. The information that has been supplied may lead to the discovery of new routes for the possible therapeutic applications of members of the *Cachrys* genus. When the findings of our research were compared with those obtained from the previous one, it was discovered that the latter demonstrated a higher level of activity.

2.5 | Inhibitory Potential of Different Extracts Obtained From *C. cristata* on Advanced Glycation End Product (AGE) Formation

Glycation is the modification of proteins, lipids, and nucleic acids as a result of nonenzymatic reactions with reducing sugars. AGEs are harmful compounds that are formed in the final stage of this process, accelerating cell aging and contributing to various degenerative diseases [47–49]. Skin aging, in particular, is directly related to factors such as ROS production caused by AGE accumulation, deterioration of enzymatic systems, and hardening of collagen cross-links [50]. AGEs have been found to trigger oxidative stress and inflammation by increasing the production of ROS, particularly through NADPH oxidase (NOX) and mitochondrial dysfunction [51, 52]. In this context, in Figure 1a, the inhibitory effects of extracts obtained from *C. cristata* plant using different solvents on AGE formation were examined. It is seen that ethyl acetate (80.71%), ethanol (75.89%), and ethanol/water (71.01%) extracts inhibit AGE formation to a high extent. The inhibitory effect of the WE (60.19%) remained at a lower level compared with other extracts. Figure 1b shows the AGE inhibition percentages of quercetin standard. AGE inhibition was highest at the highest

TABLE 4 | Enzyme inhibitory properties of the tested extracts.

Extracts	AChE (mg GALAE/g dry extract)	BChE (mg GALAE/g dry extract)	Tyrosinase (mg KAE/g dry extract)	Amylase (mmol ACAE/g dry extract)	Glucosidase (mmol ACAE/g dry extract)
Ethyl acetate	3.14 ± 0.42^{c}	$2.64 \pm 0.08^{c,d}$	38.47 ± 0.38^{c}	0.65 ± 0.03^{a}	na
Ethanol	3.55 ± 0.08^{a}	3.29 ± 0.57^{b}	40.06 ± 0.70^{b}	0.46 ± 0.01^{b}	na
Ethanol/water (70%)	3.32 ± 0.07^{b}	2.69 ± 0.32^{c}	41.26 ± 0.57^{a}	0.34 ± 0.01^{c}	1.47 ± 0.01^{a}
Water (infused)	1.26 ± 0.04^{d}	3.86 ± 0.36^{a}	9.66 ± 0.94^{d}	0.05 ± 0.01^{d}	0.11 ± 0.01^{b}

Note: Values are reported as mean ± SD of three parallel measurements. Different letters indicate significant differences among the tested extracts ($p < 0.05$).
Abbreviations: ACAE, acarbose equivalent; GALAE, galantamine equivalent; KAE, kojic acid equivalent; na, not active.

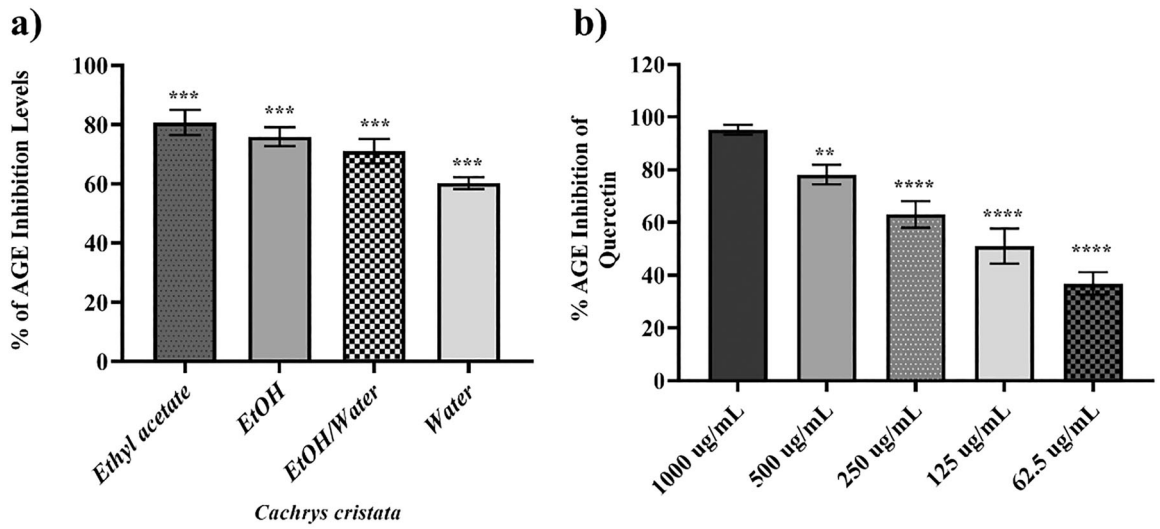

FIGURE 1 | Inhibitory effects of *Cachrys cristata* extracts on the formation of advanced glycation end products (AGEs). (a) AGE inhibition percentages of ethyl acetate, ethanol (EtOH), ethanol/water (EtOH/Water), and water extracts of *C. cristata*. (b) AGE inhibition percentages of quercetin standard at different concentrations. Results are given as mean ± standard error ($n = 3$). Statistical significance levels: $^{**}p < 0.01$, $^{***}p < 0.001$, $^{****}p < 0.0001$.

concentration (1000 μg/mL), and a dose-dependent decrease was observed. These results show that *C. cristata* extracts have anti-glycation potential, and this effect may vary depending on the composition of the extract. In particular, the ethyl acetate extract had the highest AGE inhibition, suggesting that the extract may be rich in polyphenolic compounds. The results in Figure 8 (see below), which were parallel to the amylase experiment conducted within the scope of the study and presented in Table 4, indicate that the ethyl acetate extract had the highest antidiabetic effect. On the other hand, according to the phytochemical content analyses presented in Table 2, it has been observed that *C. cristata* plays a role in AGE inhibition, especially thanks to the various chemical compounds it possesses [53, 54]. Polyphenols such as syringic acid, vanillic acid, ferulic acid, chlorogenic acid, caffeic acid, hesperidin, rutin, fisetin, morin, quercetin, luteolin, and kaempferol were found in *C. cristata* extracts. These compounds have been previously shown to contribute to AGE inhibition [55–57]. On the other hand, it has been presented in the literature that flavonoids, especially quercetin, rutin, and luteolin, can prevent the formation of AGEs at early stages by forming a carbonyl trap. Phenolic acids such as chlorogenic acid, caffeic acid, and ferulic acid can show an inhibitory effect by reducing the role of oxidative stress in AGE formation (de Paulo Farias et al., 2021). Although all extracts have high phytochemical content, the highest AGE inhibition of the ethyl acetate extract can be explained by the high galangin content of the extract [58, 59]. Galanin, a polyphenolic compound, has been found to have anticancer, strong antioxidant, and antidiabetic properties [60]. Similarly, it can be thought that ethyl acetate extract is more effective in AGE inhibition due to its high kaempferol content compared with other extracts. In this context, it has been revealed that *C. cristata* has the potential to prevent AGE formation thanks to the high phenolic compound content of the extracts (ethyl acetate > ethanol > ethanol/water > water, respectively). These effects indicate that *C. cristata* can be used to prevent diabetic complications and delay degenerative diseases related to aging.

2.6 | Determination of Nontoxic Concentration of *C. cristata* in HDF Cells With WST-1 Test and Its Role in Cell Viability

WST-1 test was used to determine the nontoxic concentration of *C. cristata* plant extracts obtained with different solvents on HDF cells and its effect on cytotoxicity [48, 61]. In the WST-1 assay, which is a method based on colorimetric measurement, four different *C. cristata* extracts were applied to HDF cells at increasing concentrations (25–200 μg/mL) for 48 h and the results were obtained [62, 63]. In this context, it was revealed that the extracts showed different degrees of inhibitory effect on cell viability depending on the concentration. While significant cytotoxicity was observed in all extracts, especially at concentrations of 200 μg/mL and above, it was determined that there was no statistically significant change in some extracts at lower concentrations (25,50,100 μg/Ml, etc.). When the phytochemical composition of the extracts is compared with the cytotoxicity profile obtained, it is seen that the solvent is a determining factor in the extract content. It has been revealed that ethyl acetate extract (Figure 2a) can inhibit cell proliferation due to its capacity to dissolve high lipophilic components, especially flavonoids, phenolic acids, and terpenoids [64, 65]. This is consistent with the determination of 43.19% cell viability at 200 μg/mL of this extract, and it was determined that the extract had a cytotoxic effect at increasing concentrations. Ethanol extract (Figure 2b) showed a moderate cytotoxicity supporting the presence of flavonoids and phenolic compounds since it may contain both polar and moderately apolar components. As a result of the analyses, it was observed that cell viability did not fall below 50% at concentrations of 25, 50, 100, 125, and 150 μg/mL, respectively, while the viability decreased to 49.99% at 200 μg/mL. Ethanol/water (Figure 2c) and WEs (Figure 2d), in which similar results were detected, exhibited a significant cytotoxicity especially at high concentrations since they may contain polyphenols, saponins, and other hydrophilic components. Ethanol/WE may have a stronger cytotoxic effect compared with WEs since it may contain moderate polar components as well as hydrophilic components. The relatively lower cytotoxicity of WE suggests that the effects of its components on cell metabolism may be milder or have antioxidant properties [50, 66]. In this context, the WST-1 test results show that the effect of phytochemicals contained in the *C. cristata* plant on cell viability varies depending on the different extraction methods of the plant, and especially phenolic compounds, flavonoids, and terpenoids may contribute to the cytotoxic effect. In line with this information, 150 μg/mL, which is the highest concentration at which cell viability below 50% was not observed in all extracts, was selected as the working concentration [67, 68].

2.7 | Assessment of Mitochondrial Reaktif Oksijen in UV-Induced HDF Cells Treated With *C. cristata* Extracts Using DCFDA Assay

To determine that UV irradiation significantly increased ROS production in HDF cells [69] and how *C. cristata* extracts modulated this situation, the DCFDA assay was used (Figure 3). UV irradiation causes cellular oxidative stress and increases the level of free radicals, especially ROS such as superoxide (O_2^-), hydroxyl radical (OH^-), and hydrogen peroxide (H_2O_2) [69, 70]. Mitochondrial ROS levels in HDF cells exposed to UV irradiation increased approximately 30-fold compared with the control group (Figure 3). However, a significant decrease in ROS levels was observed as a result of the treatment with ethyl acetate (17.39-fold), ethanol (5.26-fold), ethanol/water (8.7-fold), and water (3.71-fold) extracts of *C. cristata*, respectively. In particular, ethanol and WEs were the extracts that reduced ROS levels the most. This may be associated with the fact that these fractions contain more polyphenols, flavonoids, and coumarins [71–73]. As a result of the statistical examination, it was determined that the WE, which eliminated the highest mitochondrial ROS levels, had 10-fold more ROS inhibition compared with UV-induced HDFs. The results in Figure 3, which are compatible with Tables 1–3, can also be explained by the high phytochemical diversity and antioxidant potential of the WE. In previous studies, flavonoids such as quercetin, apigenin, and luteolin have been reported to suppress ROS production and prevent DNA damage [74, 75]. Similarly, coumarins strengthen cellular antioxidant defense by neutralizing ROS [76, 77]. The antioxidant capacity of *C. cristata* extracts has

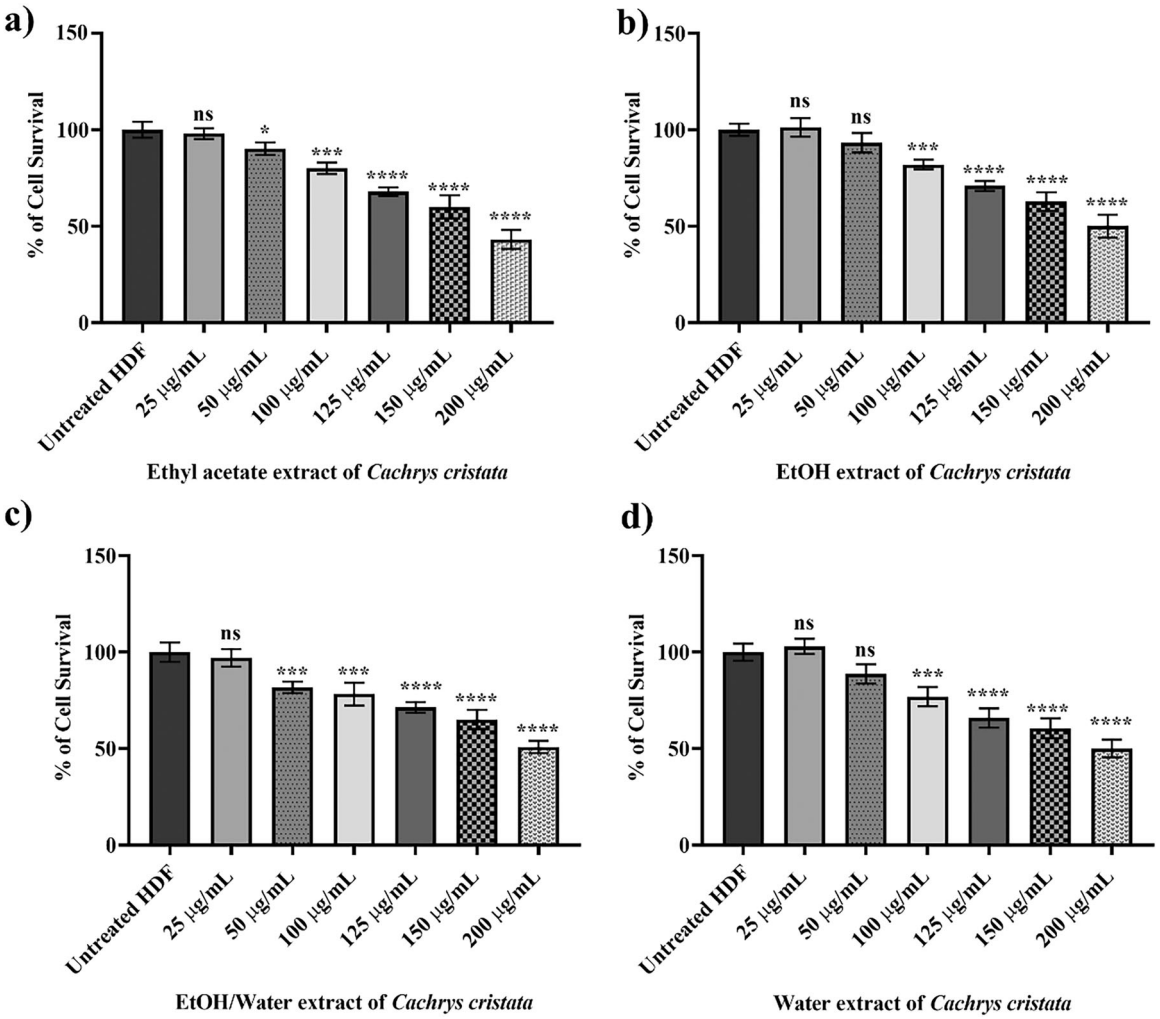

FIGURE 2 | Effects of different extracts of *Cachrys cristata* on human dermal fibroblast (HDF) cell viability. HDF cells were treated with the indicated concentrations (25–200 µg/mL) of (a) ethyl acetate extract, (b) ethanol (EtOH) extract, (c) ethanol/water (EtOH/Water) extract, and (d) water extract. Cell viability was determined using the WST-1 method. Results are expressed as mean ± standard error of the mean ($N = 3$). Statistical significance levels: ns = not significant, *$p < 0.05$, ***$p < 0.001$, ****$p < 0.0001$ (compared with the nontreated HDFs).

been demonstrated in this study to inhibit UV-induced mitochondrial ROS formation thanks to these bioactive compounds.

2.8 | Determination of Genotoxicity and UV Protective Properties of *C. cristata* Extracts on UV-Irradiated HDF Cells With COMET

Figure 4 shows that UV exposure causes DNA damage in HDF cells and the preventive effect of *C. cristata* extracts on this damage with COMET analysis. In COMET analysis, DNA damage was evaluated with the percentage of DNA carried to the tail and tail moment values. In Figure 4a, significant DNA damage is observed when HDF cells are exposed to UV. This damage is characterized by DNA tails extending outward from the cell nucleus [78–80]. However, treatment with *C. cristata* extracts reduced DNA damage. Especially ethanol and WEs provided protection by minimizing DNA damage. This may be due to the fact that these extracts are rich in polyphenols, flavonoids, and coumarins [81, 82]. UV rays increase the production of ROS in the cell, leading to oxidative stress [83]. Oxidative stress can cause oxidative modifications in DNA bases, double-stranded breaks, and the formation of protein-DNA cross-links. Such DNA damage can lead to cell death or mutations, increasing the risk of serious diseases such as cancer [84, 85]. Polyphenols and flavonoids in particular play an important role in reducing oxidative stress. For example, flavonoids (quercetin, apigenin, luteolin, etc.) reduce ROS levels by directly capturing free radicals and provide cellular protection by activating antioxidant enzymes (catalase, superoxide dismutase) [43, 86]. Coumarin derivatives can prevent DNA breaks due to oxidative stress by interacting with DNA [87, 88]. They can also limit cellular damage by inhibiting the ferroptosis mechanism [89]. Phenolic acids prevent DNA damage due to oxidative stress by neutralizing hydroxyl and superoxide radicals [90]. The antioxidant properties of these components provide protection of DNA by suppressing UV-induced ROS production. In previous studies, flavonoids such as quercetin and apigenin have been shown to significantly reduce DNA damage in COMET analysis [91, 92]. Similarly, epigallocatechin gallate (EGCG), which was used as a positive control in the experimental setup, is known to have strong antioxidant effects and increase DNA stability [80, 93]. As shown in Figure 4b,c, a significant increase in the percentage of DNA transported to the

tail and tail moment values was observed in cells exposed to UV irradiation. However, *C. cristata* extracts, especially ethanol and WEs, significantly reduced DNA damage. These findings suggest that the polyphenol and flavonoid content of *C. cristata* has the potential to prevent oxidative DNA damage and may suppress ROS-induced genotoxicity.

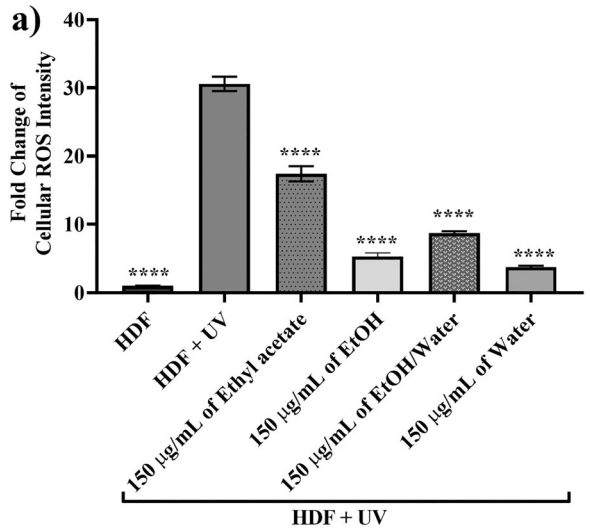

FIGURE 3 | Determination of the effects of *Cachrys cristata* extracts on UV-induced cellular ROS production by DCFDA. The changing ROS level following treatment of HDF cells with *Cachrys cristata* extracts at a concentration of 150 µg/mL after UV exposure was expressed as a fold change in fluorescence intensity. ****$p < 0.0001$ indicates the significance level.

2.9 | Determination of the Role of Different Extracts Obtained From *C. cristata* on UV-Induced Oxidative Stress Pathway by Western Blot

Figure 5 shows the levels of proteins that play a role in the effective molecular signaling pathway to add the effects of different extracts of *C. cristata* plant on UV-induced inflammatory response and oxidative stress to the literature by Western Blot method. A significant increase in phospho-NF-κB p65, AP-1, and RAGE protein expression levels was observed in HDF cells after UV exposure. This increase is directly related to the increase in ROS production in the cell by UV rays [94–96]. Increased ROS levels activate transcription factors such as NF-κB and AP-1, promoting the release of inflammatory cytokines [97, 98]. At the same time, ROS can increase RAGE expression by increasing lipid peroxidation in the cell membrane. Following UVB application to HDF cells, it was found that phospho-NF-κB p65 protein level increased by 4.95-fold, AP-1 level increased by 4.92-fold, and RAGE level increased by 5.97-fold compared with nontreated HDF cells (Figure 5b). On the other hand, following application of ethyl acetate extract of *C. cristata* plant to UV-induced HDF cells for 48 h, phospho-NF-κB p65 level decreased by 1.5-fold, AP-1 level decreased by 1.54-fold, and RAGE level decreased by 1.64-fold. Similarly,

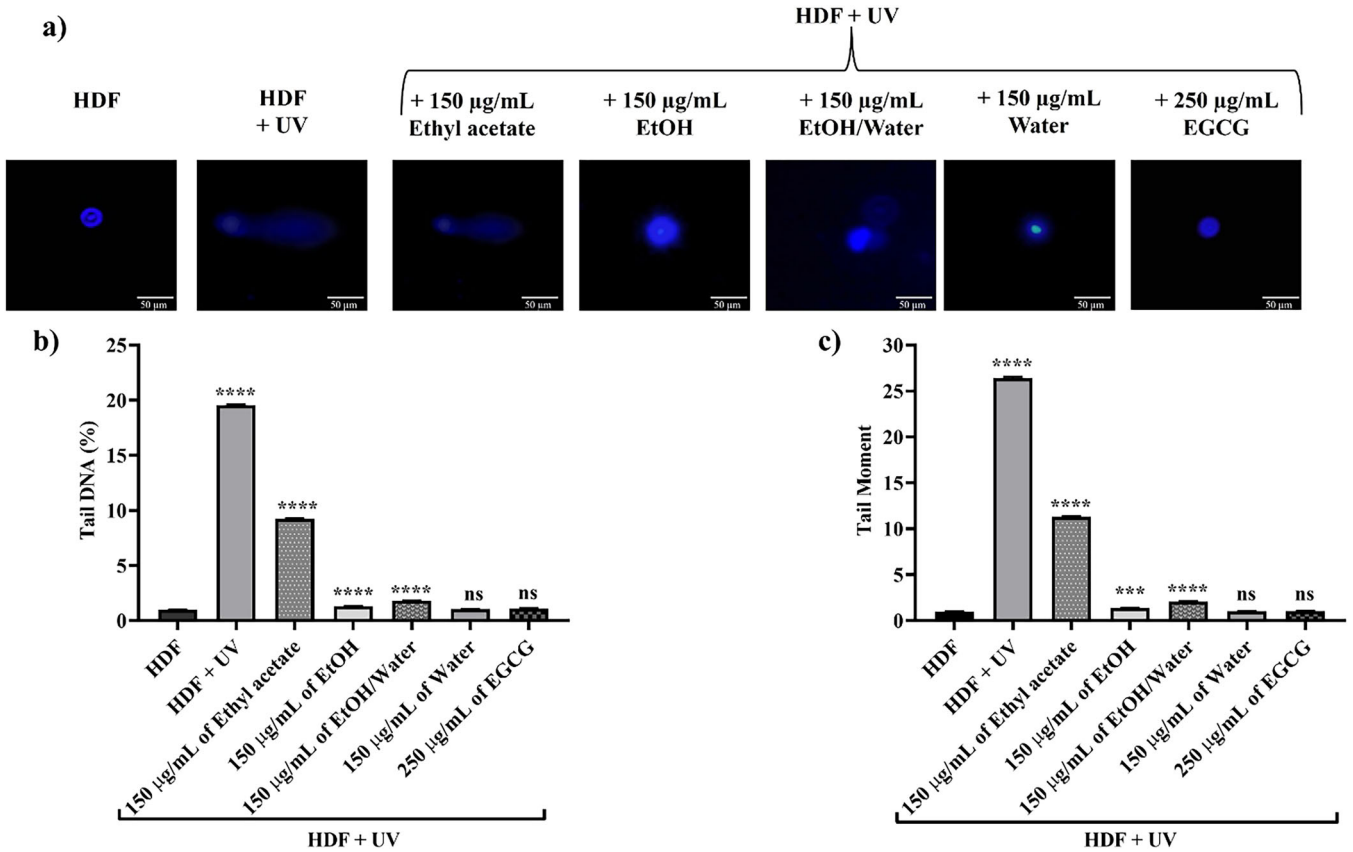

FIGURE 4 | Effects of *Cachrys cristata* extracts on UV-induced DNA damage. (a) COMET analysis images performed on HDF cells after UV exposure due to treatment with *C. cristata extracts*. (b) Tail DNA percentage (%) values. (c) Tail moment values. HDF cells were treated with 150 µg/mL *C. cristata* extracts or 250 µg/mL EGCG (positive control) after UV irradiation.

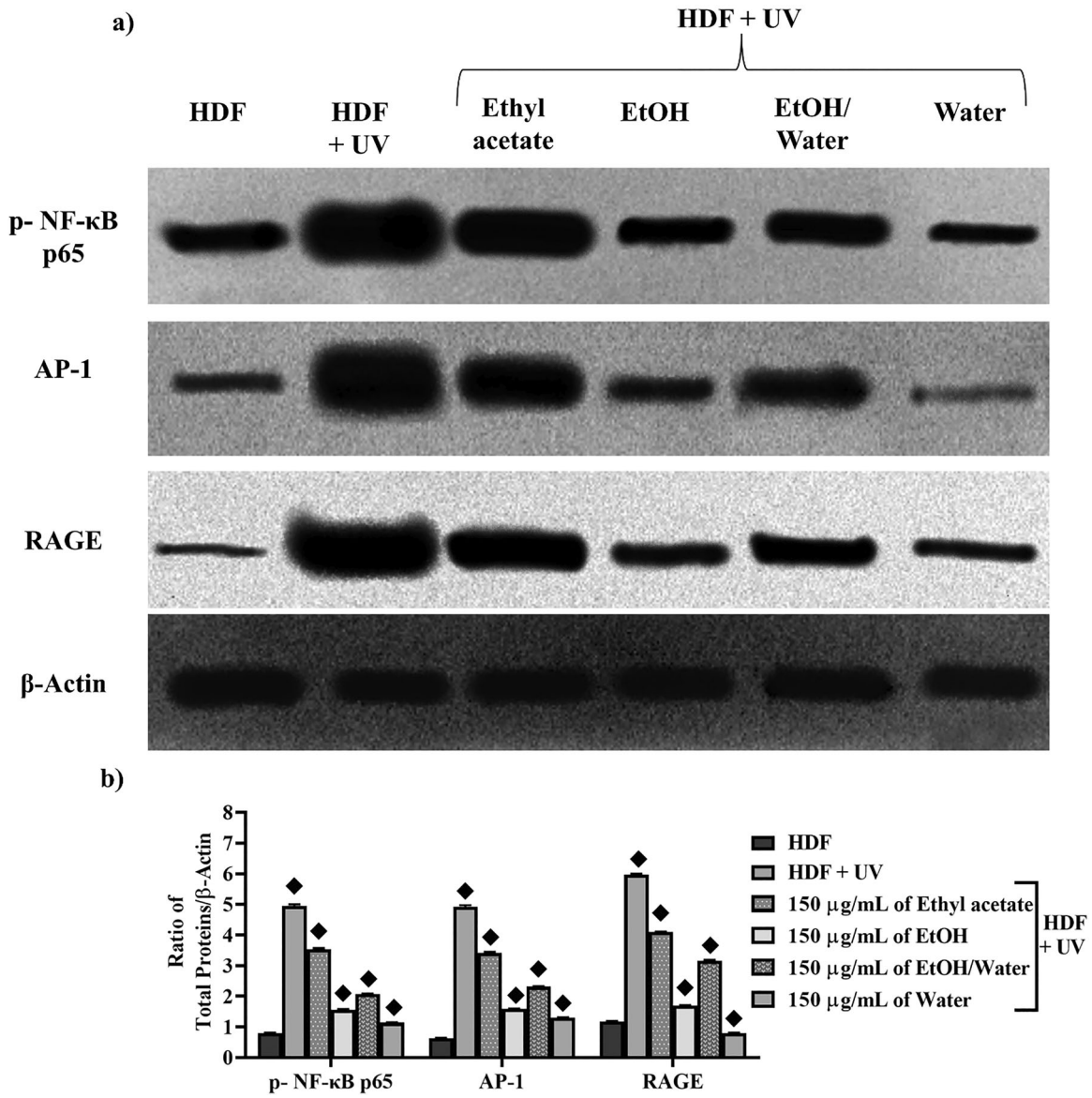

FIGURE 5 | Effects of *Cachrys cristata* extracts on the signaling pathway of UV-induced molecular damage. (a) Western blot analysis of p-NF-κB p65, AP-1, and RAGE protein expression levels in HDF cells. β-Actin was used as a loading control. (b) Quantitative analysis of Western blot band intensities of relevant proteins normalized to β-Actin. HDF cells were treated with *C. cristata* extracts at a concentration of 150 μg/mL after UV irradiation, and statistical differences of relevant proteins were made compared to untreated HDFs. $p \leq 0.0001$ was symbolized by ♦.

following application of ethanol extract, phospho-NF-κB p65 protein level decreased by 3.17-fold, AP-1 level decreased by 4.52-fold, and RAGE level decreased by 9.34-fold. After the application of ethanol/WE of *C. cristata* to UVB irradiated HDF cells, significant decreases were observed in phospho-NF-κB p65 (2.39-fold), AP-1 (2.55-fold), and RAGE (2.42-fold) protein levels, respectively, compared to UV-treated HDF cells. The *C. cristata* extract that suppressed UVB-induced ROS and related inflammation pathways at the highest level was water. It was found that the WE reduced the phospho-NF-κB p65 protein level by 4.35-fold, AP-1 level by 6.42-fold, and RAGE level by 12.65-fold, respectively (Figure 5). These effects observed in UVB irradiated-dermal fibroblasts indicate that they are due to phytochemical components such as furanocoumarins, flavonoids, and polyphenols contained in *C. cristata*. Furanocoumarins are known to inhibit proinflammatory gene expression by suppressing NF-κB pathways [99, 100]. These components ensure that NF-κB remains in the cytoplasm through the IκB kinase (IKK) complex and contribute to the reduction of inflammation and ROS levels by preventing its nuclear translocation [99, 100]. In addition, flavonoids have been shown in previous studies to reduce oxidative stress that triggers the activation of NF-κB by scavenging ROS. In addition, flavonoids suppress the inflammatory effects of NF-κB by inhibiting p38 MAPK and JNK signaling pathways [101, 102]. *C. cristata* extracts rich in polyphenols may also modulate histone deacetylase (HDAC) enzymes, reduce DNA binding of phospho NF-κB, and thus inhibit inflammatory cytokine production [103, 104]. It is thought that as a result of suppression of phospho NF-κB, synthesis of RAGE and AP-1 proteins in the downstream and upstream signaling pathways may be inhibited and the UVB-driven oxidative stress pathway may be eliminated [103]. In conclusion, *C. cristata* showed anti-inflammatory and antioxidant effects in UV-induced dermal fibroblasts and

reduced NF-κB, AP-1, and RAGE expression levels. It shows that *C. cristata* has the potential to slow down UV-induced inflammation and aging processes. Inhibition of AGE-RAGE interaction is considered an important mechanism in protecting fibroblasts against oxidative stress and suggests that it can be used against UV-induced skin damage.

2.10 | Elucidation of the Effects of *C. cristata* Extracts on Increased MMP-2 and MMP-9 Activity in UV Irradiated HDF Cells by Gelatinase Zymography

Matrix metalloproteinases (MMPs) are proteases that play a key role in the remodeling of the extracellular matrix (ECM). MMP-2 (gelatinase A) and MMP-9 (gelatinase B) are known to have the capacity to degrade basement membrane components, especially type IV collagen [105]. UV radiation has been previously shown to increase MMP expression and activity via oxidative stress [106, 107]. However, the inhibitory role of *C. cristata* in the increased MMP-2 and MMP-9 activity in UV-induced HDF cell line has not been elucidated before. In this context, UV-irradiated HDF cells were treated with four different extracts of *C. cristata* for 48 h and changes in MMP-2 and MMP-9 levels were evaluated by zymography (Figure 6). After UV exposure, MMP-9 activity increased approximately 3.5-fold and MMP-2 activity increased 2.5-fold. This shows that UV rays accelerate the degradation of the ECM by increasing ROS production. However, *C. cristata* extracts, especially water (3.54-fold decrease), ethanol (3.05-fold decrease), ethanol/water (2.35-fold decrease), and ethyl acetate (1.9-fold decrease) extracts were effective in suppressing MMP-9 activity (Figure 6a,b). Similarly, it was found that MMP-2 levels decreased 8.75-fold after the application of WE, 5.94-fold in ethanol extract, 4.12-fold in ethanol/WE, and 2.75-fold in ethyl acetate extract (Figure 6a,c). The effects of these different solvent extracts are thought to be dependent on the phytochemical content. The highest inhibitory effect of the WE highlights the effect of water-soluble phenolic compounds or flavonoids on MMP enzymes [108]. Ethanol and ethanol/WEs also provided significant inhibition, suggesting that polyphenols and other phytochemicals with high solubility in these solvents may also be effective in this process. On the other hand, the lowest inhibitory effect of the ethyl acetate extract indicates that lipophilic compounds may have lower effectiveness in terms of inhibiting MMP activity. In conclusion, the fact that extracts

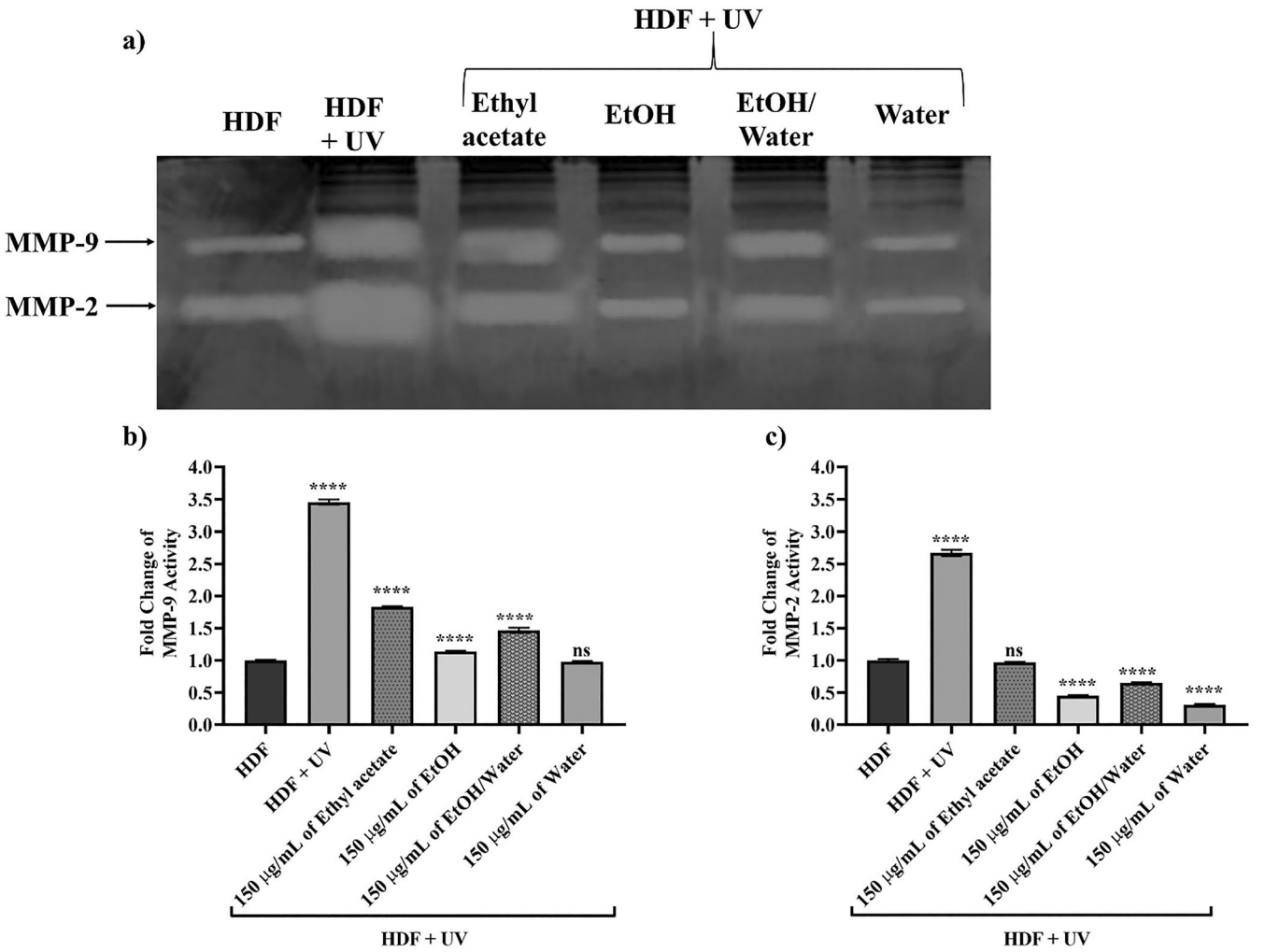

FIGURE 6 | The role of *Cachrys cristata* extracts on UV-induced MMP-2 and MMP-9 activity. (a) Gelatin zymography gel image visualizing MMP-2 and MMP-9 activity. (b) Quantitative data of fold change in MMP-9 activity. (c) Quantitative data of fold change in MMP-2 activity. **** indicates $p < 0.0001$ significance level.

obtained from *C. cristata* inhibited MMP-2 and MMP-9 activity indicates that this plant can be evaluated as a potential protective agent against UV-induced skin damage. The high effectiveness of the WE, in particular, revealed that the role of hydrophilic phytochemicals in MMP inhibition may be more dominant [109, 110]. Therefore, it has been demonstrated that water and other extracts obtained from *C. cristata* may be natural ECM modulators.

2.11 | Role of Extracts From *C. cristata* on Enzymes Responsible for Aging and Skin Barrier Homeostasis

The ECM is composed of important biomolecules that provide the integrity, elasticity, and water retention capacity of skin tissue [111]. Elastin, collagen, and hyaluronic acid are the main components of the ECM, supporting the skin structure and maintaining a youthful and healthy appearance [112, 113]. However, environmental stress factors such as ultraviolet (UV) radiation can trigger biochemical processes that threaten the integrity of the ECM. UV rays increase the production of ROS in skin cells, creating oxidative stress. This oxidative stress activates intracellular signaling pathways, resulting in the overexpression of enzymes such as MMPs, elastase, collagenase, and hyaluronidase [114, 115]. Elastin is an enzyme that causes loss of skin elasticity, and its presence causes skin sagging and accelerates the aging process [116]. Similarly, collagenase disrupts the structural integrity of the skin by causing collagen destruction [117]. Hyaluronidase enzyme breaks down hyaluronic acid, causing the skin to lose its moisture balance and fullness [118]. In parallel with this information presented in the literature, the synthesis of these enzymes at basal levels may help prevent rapid deterioration of the ECM and delay skin aging. Experiments presented in Figure 7 were conducted to test the inhibitory potential of *C. cristata* extracts on these enzymes. As a result of the statistical analyses, it was determined that the anti-collagenase activity was highest in water (88.57%) > EtOH (84.83%) > EtOH/Water (79.94%) and ethyl acetate (71.29%), respectively. The inhibitory activity of EGCG at a concentration of 250 μg/mL, used as a positive control, was calculated as 91.18% (in Figure 7a). Similar results were observed in the anti-elastase activity presented in Figure 7b, and the highest inhibitory activity was exhibited by the WE at a rate of 85.92%. The lowest activity was found in the ethyl acetate extract at a rate of 70.14%, and the inhibition value of EGCG used as a positive control was 93.37%. In anti-hyaluronidase activity, the highest values were found as water (84.79%) > EtOH (78.62%) > EtOH/Water (66.27%) and ethyl acetate (61.93%),

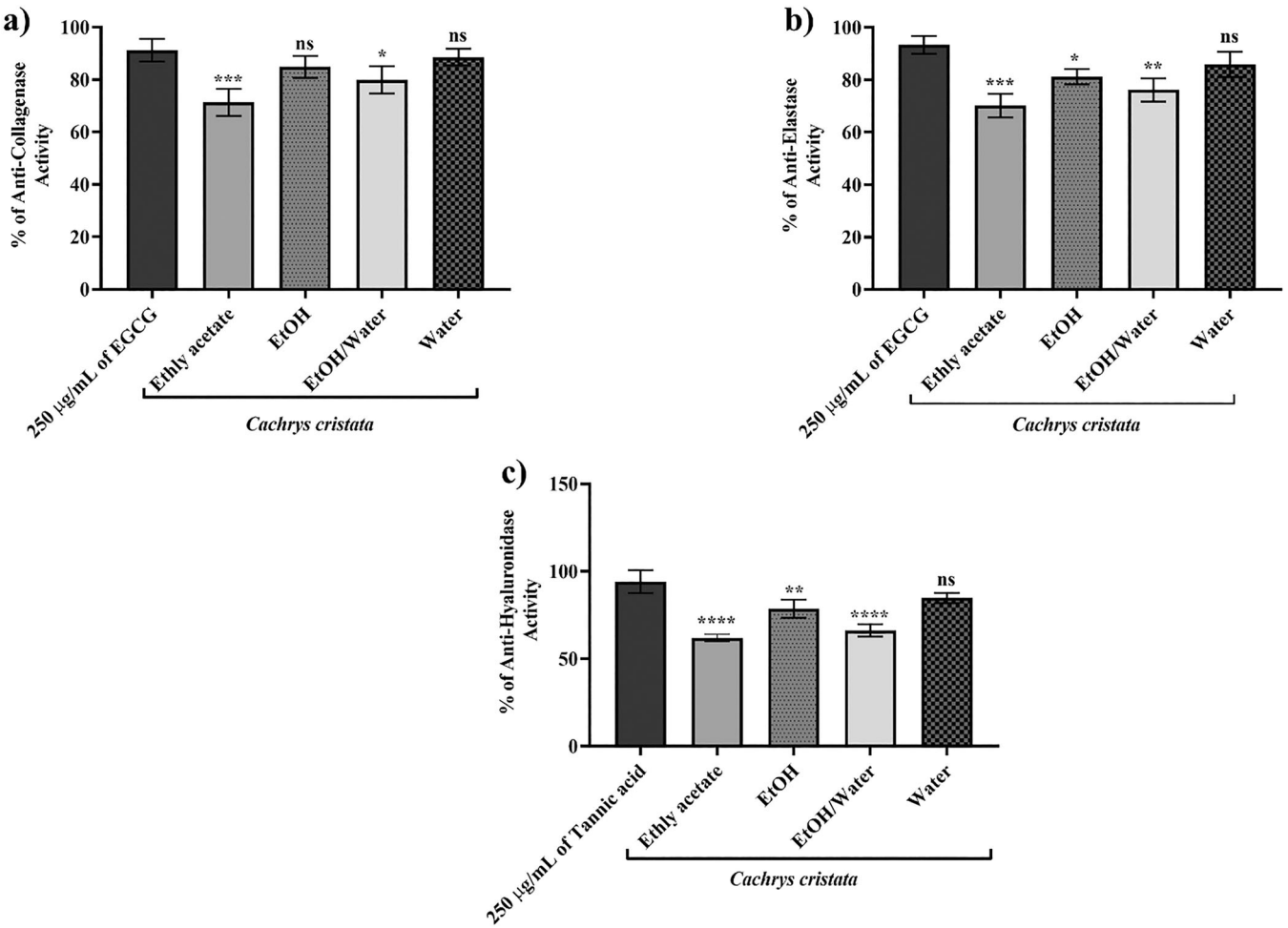

FIGURE 7 | Inhibitory effects of *Cachrys cristata* extracts on skin-associated enzymes. (a) Anti-collagenase activity (%), (b) anti-elastase activity (%), and (c) anti-hyaluronidase activity (%). 250 μg/mL of epigallocatechin gallate (EGCG) and tannic acid were used as positive controls. Statistical significance levels are indicated as follows: $*p < 0.05$, $**p < 0.01$, $***p < 0.001$, $****p < 0.0001$, ns: not significant.

respectively. The inhibitory activity of tannic acid at a concentration of 250 μg/mL used as a positive control was calculated as 94.05% (Figure 7c). In addition to the information presented, we obtained results supporting the findings in Table 2 and Figure 6. In Figure 7, it was determined that the WE exhibiting the highest inhibitory activity exhibited enzyme inhibition thanks to its bioactive compounds such as high flavonoids (quercetin, luteolin, and apigenin), phenolic acids (caffeic acid and ferulic acid), and coumarins [108, 119]. In light of this information, it has been revealed that *C. cristata* is a natural source that delays skin aging by inhibiting elastase, collagenase, and hyaluronidase enzymes thanks to the flavonoids, phenolic acids, and coumarins that all extracts have. Thus, it has been clarified that *C. cristata* can both protect against UV-induced damage and prevent the destruction of structural proteins in the dermal matrix. Thanks to the synergistic effect of these compounds, this study has indicated that phytochemical-rich plants such as *C. cristata* have significant potential in antiaging cosmetic and pharmaceutical products.

2.12 | Network Pharmacology

The present study focused on the phytochemicals of *C. cristata*, including caffeic acid, quercetin, syringin, catechin, and rutin. The gene targets of these compounds were identified through an analysis of the Comparative Toxicogenomics Database (CTD) and the PubChem database. Nodes with a degree value of 2 or higher were selected for further analysis, and the results were validated using the STRING plugin. Consequently, 443 gene targets and 984 edges were identified (Figure 8a). The results of the PPI analysis offered significant insights into the potential biological functions of the genes that exhibited overlap. These findings contribute to a more profound comprehension of the target proteins of these molecules and establish a foundation for future research in this field. A gene interaction network comprising 380 nodes and 89,56 edges was identified through analysis of the STRING database. The maximal clique centrality (MCC) method, implemented through the CytoHubba plugin, was employed to identify key hub genes, including IL6, TNF, ACTP, and INS (Figure 8b).

The Disease Ontology Enrichment (DOSE) analysis revealed significant correlations between the analyzed genes and a multitude of diseases. Notable enrichments included hepatitis, ischemia, and liver cirrhosis, followed by diseases such as musculoskeletal system cancer, connective tissue cancer, and cardiovascular conditions, including arteriosclerosis, atherosclerosis, and myocardial infarction. Furthermore, associations were identified with chronic obstructive pulmonary disease (COPD), lysosomal storage disease, and other systemic conditions,

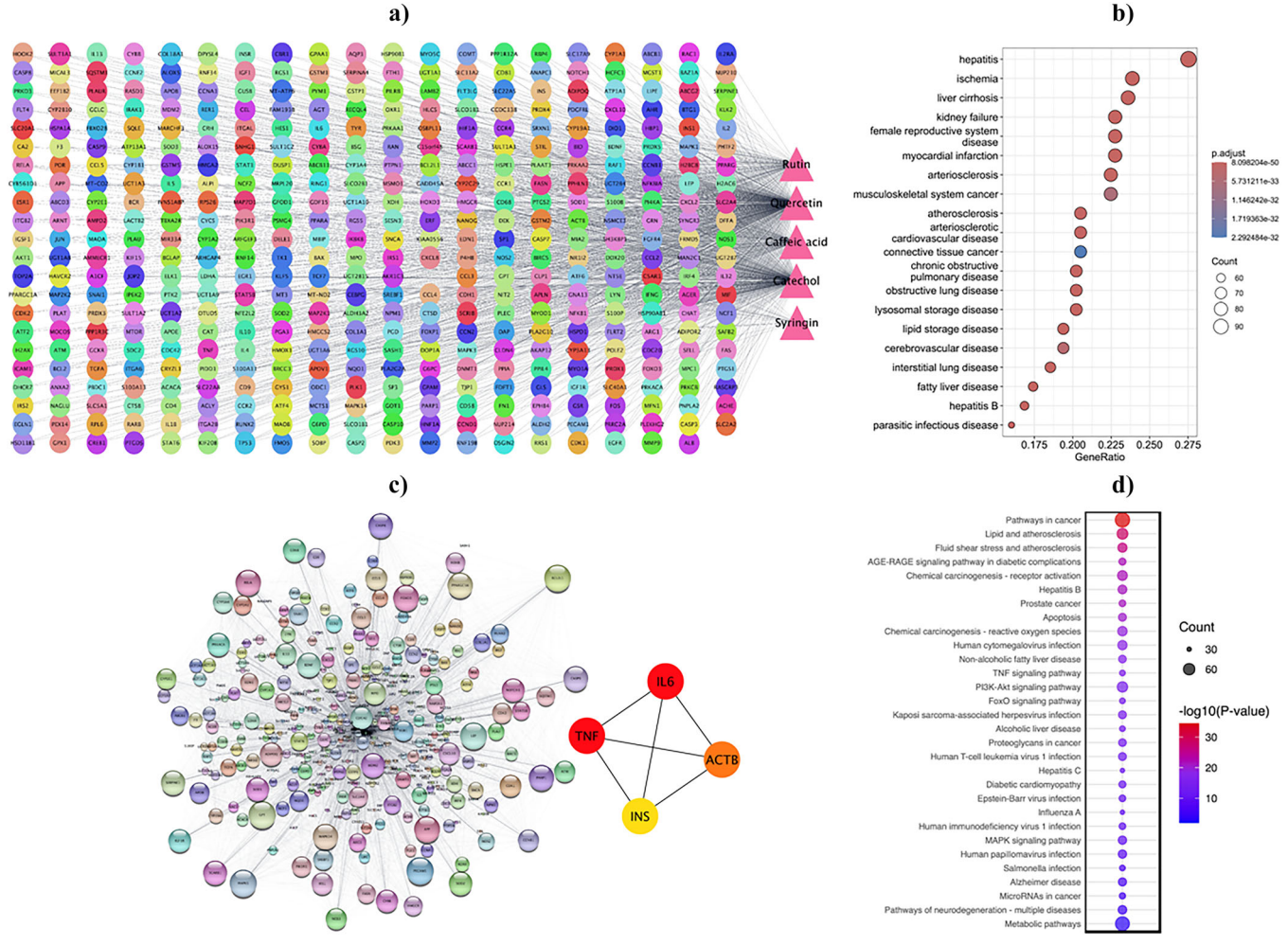

FIGURE 8 | Network pharmacology workflow: (a) Target analysis of *Cachrys cristata* compounds. (b) DOSE analysis illustrating the association between genes and diseases. (c) Gene overlap related to *Cachrys cristata*. (d) KEGG pathway enrichment analysis of disease-related terms.

including female reproductive system disease and kidney failure. These results indicate the broad biological relevance of the investigated genes across multiple disease pathways, particularly in cancer, cardiovascular, and liver-related disorders. The findings provide a more profound comprehension of the molecular mechanisms that underpin these diseases and underscore the potential functional roles of the genes within a multitude of pathological processes (Figure 8c).

A target-pathway enrichment analysis conducted using the DAVID database yielded crucial insights into the potential biological impacts of *C. cristata* components. The analysis revealed significant enrichment across 188 pathways ($p < 0.05$), thereby underscoring the extensive therapeutic and biological potential of the plant's bioactive compounds. Among the enriched pathways, several are directly associated with cancer biology, including "Pathways in Cancer," "Proteoglycans in Cancer," and "MicroRNAs in Cancer." These pathways are fundamental to processes such as tumor development, metastasis, and cellular signaling. Furthermore, pathways associated with essential cellular mechanisms, including apoptosis, oxidative stress responses, and inflammatory regulation, were significantly enriched, indicating the extensive mechanistic impact of *C. cristata* components. Furthermore, the findings indicated significant associations with critical signaling pathways, including the PI3K-Akt and MAPK signaling pathways, which regulate cell survival, proliferation, and apoptosis. These pathways are not only central to cancer progression but also integral to metabolic and inflammatory diseases, further emphasizing the multifaceted potential of *C. cristata*. The enrichment of these interconnected pathways suggests that the bioactive compounds in *C. cristata* can target multiple molecular and cellular processes simultaneously. This highlights their potential as versatile therapeutic agents capable of influencing a wide range of biological functions and disease states. Collectively, the results point to *C. cristata* as a promising candidate for future research into its biomedical applications (Figure 8).

2.13 | Molecular Docking Results

The binding energy scores show that rutin, quercetin, and syringin have the highest binding propensity for AChE, BChE, amylase, and collagenase, while rutin and quercetin demonstrate the strongest binding to MMP-2 and MMP-9 (Figure 9). For example, protein–ligand interaction analysis shows that rutin binds to both AChE and BChE mainly via multiple H-bonds and several hydrophobic interactions, with π–π stacking interaction unique to AChE complex (Figure 9a) and metal–acceptor interaction with the Zn^{2+} ion in the active site of BChE (Figure 9b). In addition, several van der Waals interactions were formed with mainly polar residues lining the active sites of the two enzymes (Figure 10a,b). Trp286, found to form a hydrophobic interaction in the AChE complex with rutin, is one of the essential residues for the catalytic activity AChE [120]. Similarly, His438, which is found to be engaged in van der Waals interaction here, is a member of the catalytic triad (Ser198, Glu325, and His438) of BChE. Interestingly, syringin displays a plausible binding mode in the catalytic pocket of tyrosinase, amylase, and glucosidase (Figure 10c–e). H-bonds are the key interactions in the tyrosinase complex with syringin, while van der Waals interactions reinforce the binding (Figure 10c). His363 and His367, which were involved in the formation of van der Waals interaction, are among the seven conserved histidine residues that are essential for tyrosinase activity [121]. Similarly, H-bonds play a critical role in the interaction of syringin with amylase and glucosidase, while multiple hydrophobic contacts contribute to the binding strength of the ligand (Figure 10d,e). In particular, most of the interactions formed by syringin with amylase are also present in the amylase-acarbose crystal complex [122]. Furthermore, the binding of rutin to elastase, collagenase, and hyaluronidase is demonstrated in the 2D interaction diagrams, in which multiple H-bonds with mainly polar active site residues are the key interactions (Figure 11a–c). While van der Waals and hydrophobic interactions reinforce the binding of rutin to elastase (Figure 11a), both interactions coupled with metal–acceptor

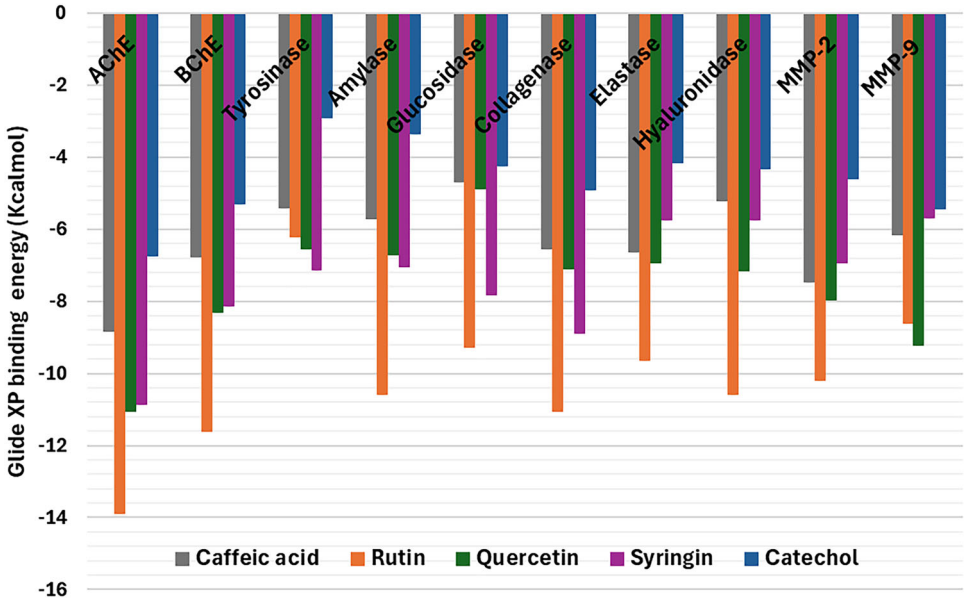

FIGURE 9 | Glide XP binding energy scores of the bioactive compounds in the extract of the aerial parts of *Cachrys cristata*.

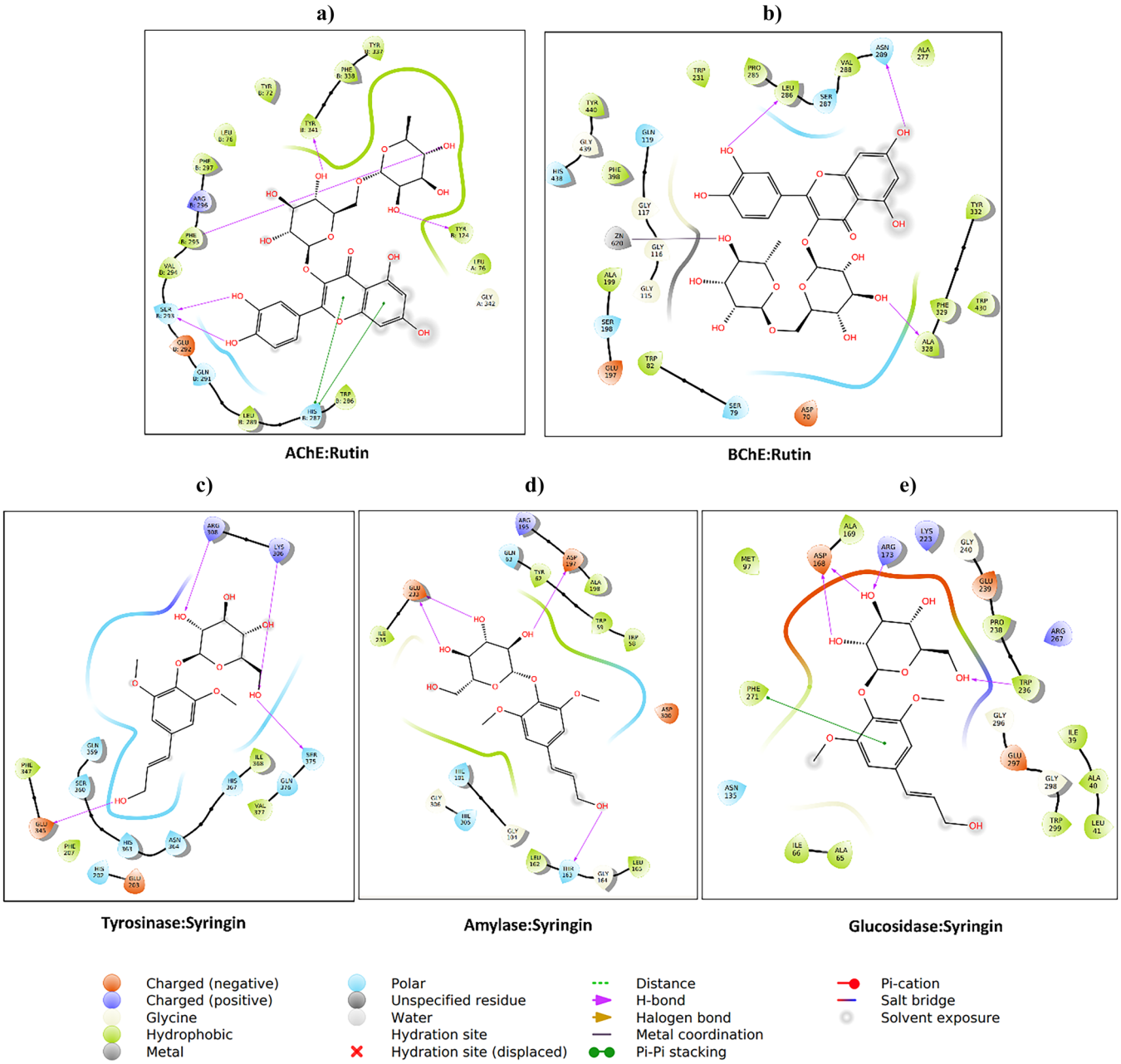

FIGURE 10 | Protein–ligand interaction: (a) AChE and rutin, (b) BChE and rutin, (c) tyrosinase and syringin, (d) amylase and syringin, and (e) glucosidase syringin.

interactions between active site Zn^{2+} ion and OH group contribute to the binding of rutin to collagenase (Figure 11b). In addition to van der Waals and hydrophobic interactions, rutin formed a π–cation interaction with Lys127 via the quercetin moiety (Figure 11c). A member of the catalytic triad (H71, D119, and S214) of elastase, His214 is involved in forming van der Waals interaction with rutin, suggesting possible enzyme inhibition [123]. Moreover, the inhibition of collagenase may be achieved by blocking the active site Zn^{2+} ion [124]. Quercetin is completely accommodated in the active site cavity of MMP-2 and interacts mainly via H-bonds and hydrophobic contacts, and a π–π stacking interaction with His226 (Figure 11d). Finally, the binding of rutin to another cancer protein target MMP-9 is through a combination of 2 H-bonds with the backbone of Ala, multiple hydrophobic contacts, a few van der Waals, and π–anion and metal–acceptor interactions, both with the active site Zn^{2+} ion (Figure 11e). The most common mode of action of MMP inhibitors is binding to the Zn^{2+} ion in the active site of MMP enzymes to block the functioning of the metal ion [125].

2.14 | Binding Free Energy Analysis: Molecular Mechanics/Poisson-Boltzmann Surface Area (MM/PBSA) Results and Implications for Ligand Efficacy

This study sought to investigate the stability and binding efficacy of various protein–ligand complexes through the use of MM/PBSA binding free energy calculations, which were integrated with MD simulations. The key energy parameters evaluated included van

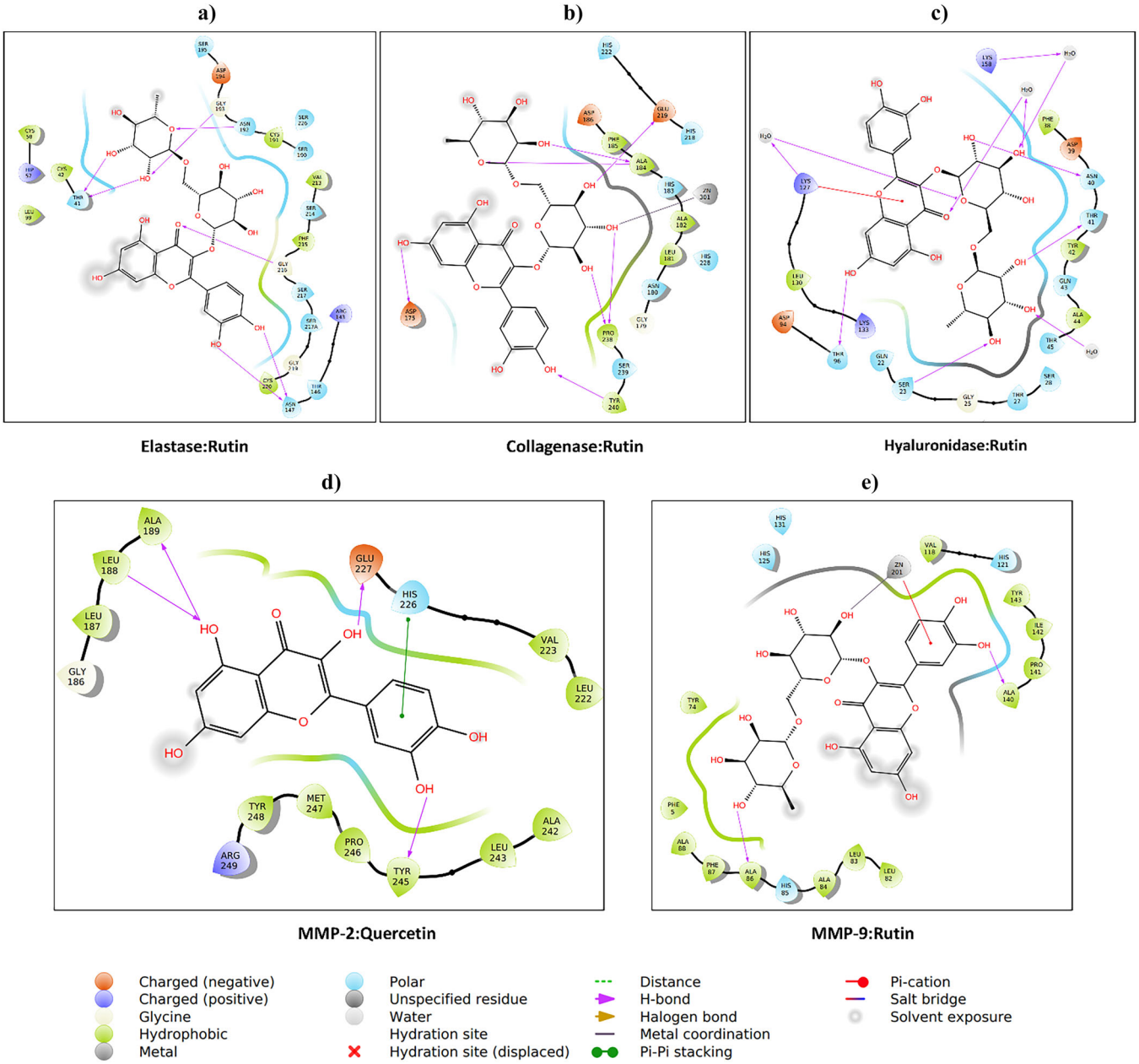

FIGURE 11 | Protein–ligand interaction: (a) elastase and rutin, (b) collagenase and rutin, (c) hyaluronidase and rutin, (d) MMP-2 and quercetin, and (e) MMP-9 and rutin.

der Waals interactions (VDWAALS), electrostatic energy (EEL), polar solvation energy (EGB), surface tension (ESURF), gas-phase energy (GGAS), solvation energy (GSOLV), and total binding energy (TOTAL). The enzymatic activities of MMP-9, MMP-2, AChE, BChE, collagenase, and hyaluronidase in complex with compounds derived from *C. cristata* were analyzed. Based on the following criteria: RMSD, high binding energy, and the number of hydrogen bonds formed, three complexes were selected for further investigation. The complexes identified as worthy of further investigation, namely Quercetin_MMP-9, Rutin_BChE, and Rutin_MMP-2, are highlighted in Table S1 and depicted in Figure 12.

The analysis identified Quercetin_MMP9 (total energy = −34.65 kcal/mol), Rutin_BChE (total energy = −52.64 kcal/mol), and Rutin_MMP2 (total energy = −24.51 kcal/mol) as the most promising candidates for MD simulations (Figure 9). These complexes were prioritized due to their favorable total energy values, stable binding profiles, and strong contributions from key interaction components, including van der Waals forces and electrostatic energies (Table S1). For example, Quercetin_MMP9 exhibited notable stability, as evidenced by a van der Waals contribution (VDWAALS) of −41.28 kcal/mol and an electrostatic component (EEL) of −30.05 kcal/mol. Notwithstanding a favorable solvation energy (GSOLV = 36.68 kcal/mol), the robust gas-phase energy (GGAS = −71.33 kcal/mol) yielded an overall favorable binding energy (Figure 12a). Similarly, Rutin_BChE exhibited the most robust binding characteristics among all tested complexes, with a total energy of −52.64 kcal/mol. This complex exhibited substantial electrostatic interactions (EEL = −67.68 kcal/mol) and a markedly favorable GGAS value of −120.01 kcal/mol, indicative of strong

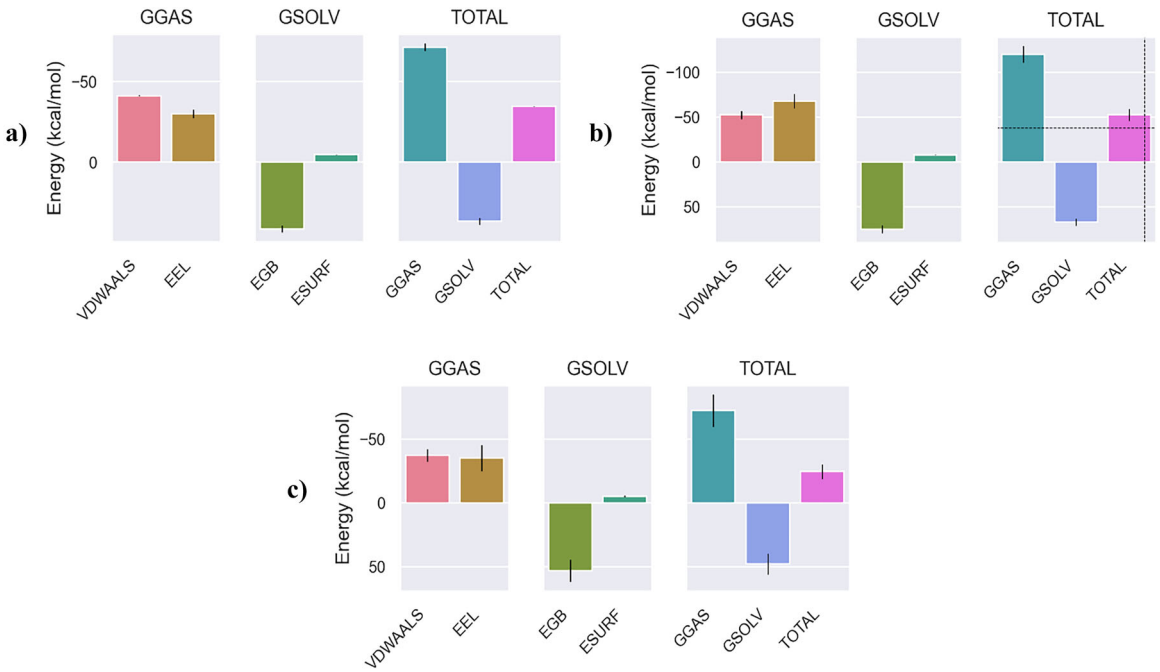

FIGURE 12 | MM/PBSA binding free energy analysis. (a) Quercetin_MMP-9 complex. (b) Rutin_BChE complex. (c) Rutin_MMP-2 complex.

and stable binding within the active site (Figure 12b). While Rutin_MMP2 exhibited slightly reduced binding potential in comparison to the other two complexes, it displayed significant affinity, as indicated by a VDWAALS value of −37.33 kcal/mol and an EEL contribution of −35.12 kcal/mol (Figure 12c). The remaining complexes, including Rutin_Collagenase (total energy = −22.74 kcal/mol) and Rutin_AChE (total energy = −3.46 kcal/mol), exhibited moderate binding affinities. While these complexes benefited from favorable van der Waals and solvation contributions, higher energy fluctuations and weaker electrostatic interactions resulted in reduced overall stability. The Rutin_Hyaluronidase complex exhibited the lowest binding potential (total energy = −1.22 kcal/mol), with minimal van der Waals interactions (VDWAALS = −3.5 kcal/mol) and poor electrostatic stability, rendering it the least promising candidate (Table S1). These findings underscore the importance of balancing van der Waals forces, electrostatic interactions, and solvation energies to achieve optimal ligand binding. Consequently, Quercetin_MMP9, Rutin_BChE, and Rutin_MMP2 were identified as the most promising candidates for further MD simulations and therapeutic exploration, owing to their superior energy profiles and stable interaction characteristics.

2.15 | Stability and Flexibility in MD Simulation

The primary objective of this study is to identify potential therapeutic drugs through a detailed investigation of the molecular interactions between selected ligands and target proteins, with a particular emphasis on elucidating their binding sites. Among the evaluated complexes, Quercetin_MMP-9, Rutin_BChE, and Rutin_MMP-2 complexes were identified as key candidates for further analysis. These complexes exhibited strong selectivity and stability in their interactions, meeting critical criteria such as the presence of hydrogen-bonding residues and favorable results from MM/PBSA binding free energy calculations. Subsequently, MD simulations were conducted to provide deeper insights into their biological efficacy and protein-binding capacities. These simulations enabled a more comprehensive evaluation of their potential as therapeutic agents, highlighting their suitability for further drug development efforts.

The structural stability of three distinct ligand–protein complexes was evaluated through the analysis of their RMSD values, obtained from MD simulations conducted over 100 ns. The Rutin_MMP-2 complex exhibits notable structural variability, with RMSD values fluctuating between 0.4 and 0.8 nm throughout the simulation. In comparison to the other complexes, it exhibits a lower degree of structural stability, as evidenced by its elevated fluctuations. In contrast, the Quercetin_MMP-9 and Rutin_BChE complexes exhibit more stable structural conformations, with RMSD values consistently ranging between 0.1 and 0.3 nm for Quercetin_MMP-9 and 0.2 to 0.35 nm for Rutin_BChE. The observation of stable RMSD profiles for these two complexes throughout the simulation period indicates that they maintain structural integrity within their binding regions, which may contribute to stronger interactions with their respective targets. In conclusion, the Quercetin_MMP-9 and Rutin_BChE complexes display greater structural stability with lower RMSD values in comparison to the Rutin_MMP-2 complex. These findings suggest that the Quercetin_MMP-9 and Rutin_BChE complexes are more stable and exhibit greater integrity within their binding regions compared to the Rutin_MMP-2 complex (Figure 13a). The RMSF plot is a useful tool for illustrating the flexibility of residues in protein complexes. The Rutin_BChE and Quercetin_MMP-9 complexes exhibit low flexibility across the majority of residues, particularly between residues 1–300, where both complexes demonstrate relatively stable structures. Minor increases in flexibility are observed in specific regions, such as residues 112–177 in the Quercetin_MMP-9 complex, with a peak value of 0.867 nm, and

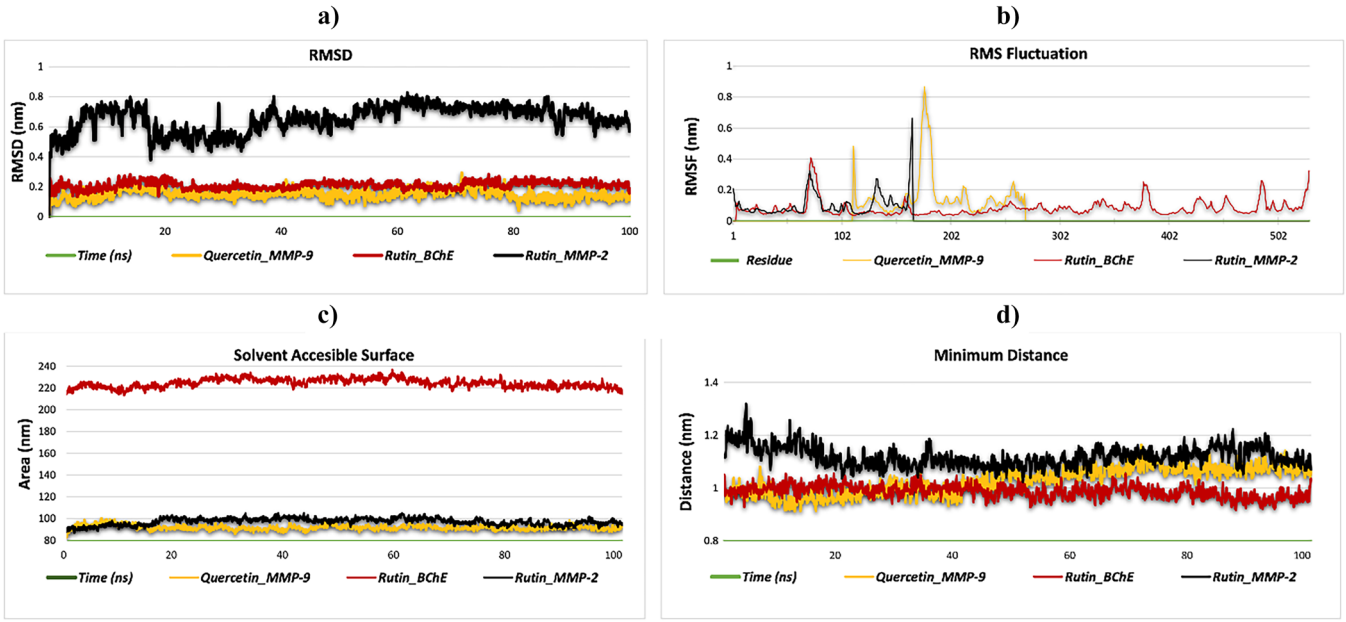

FIGURE 13 | Presentation of molecular dynamics simulations in graphical form; (a) RMSD of Quercetin_MMP-9, Rutin_BChE, and Rutin_MMP-2 complexes. (b) RMSF of Quercetin_MMP-9, Rutin_BChE, and Rutin_MMP-2 complexes. (c) Solvent Accessibility of Quercetin_MMP-9, Rutin_BChE, and Rutin_MMP-2 complexes. (d) Minimum distance of Quercetin_MMP-9, Rutin_BChE, and Rutin_MMP-2 complexes.

residues 70–78 in the Rutin_BChE complex, where the RMSF values reach 0.4086 nm. These observations indicate that these regions are not directly involved in the binding conformation. In contrast, the Rutin_MMP-2 complex displays notable increases in flexibility, particularly between residues 67–75 and 112–135, with RMSF values reaching 0.3263 and 0.6652 nm, respectively. These pronounced fluctuations suggest that the protein exhibits heightened flexibility in regions remote from the binding site, which may render it more susceptible to structural alterations. In general, the RMSF observed in the Rutin_BChE and Quercetin_MMP-9 complexes indicates a more stable structural configuration, with reduced flexibility in the binding regions. In contrast, the Rutin_MMP-2 complex exhibits enhanced flexibility in specific regions, suggesting the presence of dynamic conformational changes in these areas (Figure 13b). The solvent exposure of the ligand–protein complexes was evaluated through the SASA method over a 100 ns simulation period. The Rutin_BChE complex exhibited the highest solvent accessibility, with an average SASA value of approximately 220 nm^2, indicating substantial solvent interaction and a larger exposed surface area. This extensive interaction may be indicative of a dynamic and flexible conformation for this complex. In contrast, the Rutin_MMP-2 complex exhibited moderate SASA values, with an average of approximately 100 nm^2, indicating a more compact structure with limited solvent exposure. The diminished solvent interaction in this complex may be indicative of a stable and tightly packed conformation. The Quercetin_MMP-9 complex exhibited the lowest SASA values, averaging approximately 90 nm^2, which suggests a highly compact and solvent-isolated structure. This low SASA value may contribute to the overall stability and reduced flexibility of the complex within the binding pocket. In conclusion, the Rutin_BChE complex displays higher SASA values, indicating extensive solvent interaction, while the Quercetin_MMP-9 complex exhibits a low SASA, suggesting a compact and stable structure. The Rutin_MMP-2 complex exhibits a moderate degree of solvent exposure, situated between the other two complexes in terms of solvent interaction. These observations underscore the potential impact of solvent accessibility on the structural stability and dynamics of the complexes (Figure 13c). The minimum distance between atoms in the binding region provides insights into the structural stability of ligand–protein complexes. The Quercetin_MMP-9 complex displays moderate fluctuations in the minimum distance, with values ranging between 0.95 and 1.08 nm throughout the simulation. This indicates notable mobility in the binding region. However, this mobility remains relatively constant, indicating that the complex displays moderate flexibility in its binding conformation. In contrast, the Rutin_BChE complex exhibits greater stability, with the minimum distance consistently ranging between 0.93 and 1.04 nm. This behavior indicates a more compact and stable binding conformation, with minimal fluctuations in the binding region. The Rutin_MMP-2 complex displays more pronounced fluctuations, with the minimum distance varying between 1.05 and 1.20 nm. These results indicate that the Rutin_BChE complex exhibits greater flexibility and dynamic behavior in its binding conformation compared to the other complexes (Figure 13d).

During the 100-ns simulation of the Quercetin_MMP-9 complex, the number of hydrogen bonds exhibited fluctuations between a minimum of 0 and a maximum of 6 (Figure 14a). During the initial 20 ns, the hydrogen bond count exhibited significant fluctuations, ranging from 1 to 5, indicating a dynamic adaptation phase of the ligand within the binding site. As the simulation proceeded from 20 to 60 ns, a relatively stable pattern emerged, with the number of bonds fluctuating between two and four. In the final stages of the simulation (60–100 ns), the number of hydrogen bonds exhibited minor fluctuations between 1 and 5. This trend indicates that the binding interactions within this complex were moderately stable, with dynamic behavior persisting throughout the simulation. In the case of the Rutin_BChE complex, the number of hydrogen

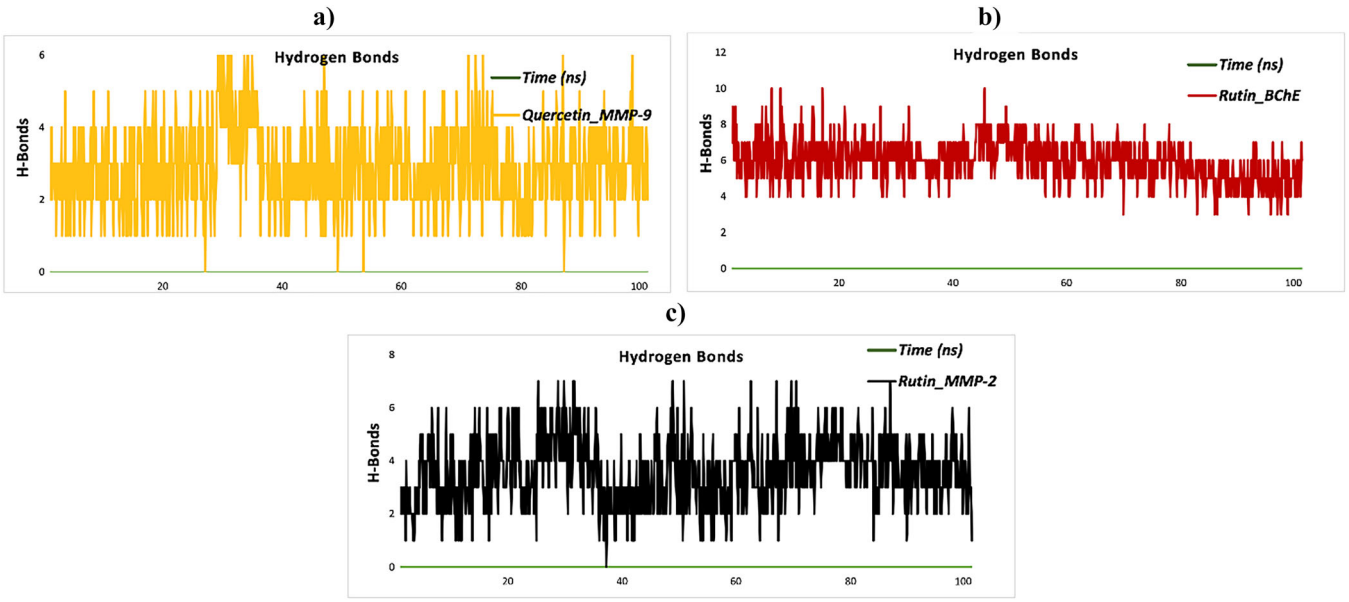

FIGURE 14 | Hydrogen bond analysis of ligand–protein complexes over a 100-ns simulation period. (a) Hydrogen bonds in the Quercetin_MMP-9 complex. (b) Hydrogen bonds in the Rutin_BChE complex. (c) Hydrogen bonds in the Rutin_MMP-2 complex.

bonds demonstrated a fluctuating pattern, with a range of 4–10 throughout the simulation (Figure 14b). During the initial 20 ns, the number of hydrogen bonds exhibited notable fluctuations between 6 and 9, indicating that the ligand was undergoing a process of adaptation to the binding site. Between 20 and 60 ns, the number of hydrogen bonds remained relatively stable, fluctuating between 5 and 7, indicative of robust and consistent binding interactions. In the final stages (60–100 ns), the hydrogen bond count remained stable within the range of 5–7, indicating that the binding remained robust over time. With regard to the Rutin_MMP-2 complex, the number of hydrogen bonds exhibited considerable variation, ranging between one and seven throughout the course of the simulation (Figure 14c). During the initial 20 ns, the number of hydrogen bonds exhibited significant fluctuations, ranging from 2 to 6. This indicates that the ligand was undergoing dynamic interactions as it adapted to the binding site. Between 20 and 60 ns, the number of hydrogen bonds stabilized at a range of 3–5, indicating the formation of a consistent interaction network. Nevertheless, in the final stages (60–100 ns), a slight increase in variability was observed, with the number of hydrogen bonds ranging between 2 and 6. This suggests that, while the complex retained its binding interactions, some degree of dynamic behavior persisted. These findings suggest that the Rutin_BChE complex exhibited the most stable hydrogen bond interactions among the three complexes, which is indicative of its strong binding potential. In contrast, the Quercetin_MMP-9 and Rutin_MMP-2 complexes exhibited moderate stability, with varying degrees of dynamic behavior in their binding interactions.

3 | Conclusion

This study conducted a comprehensive analysis of extracts obtained from *C. cristata*, evaluating their capacities to inhibit enzymes and serve as antioxidants. Various extraction solvents were employed to extract and identify the most bioactive extracts and chemicals from this plant. The ethanol, WEs showed increased concentrations of polyphenols and flavonoids, demonstrating higher antioxidant activities. Furthermore, network pharmacology analyses in conjunction with in silico molecular docking and MD simulations offered insight into the potential molecular targets and mechanisms of these phytoconstituents, thereby reinforcing their therapeutic significance. These extracts show promise as enzyme inhibitors, paving the way for nutraceutical development. Furthermore, these extracts obtained from plants have shown promise as valuable sources of enzyme inhibitors associated with different human problems. This paves the way for further investigation into their possible use in the creation of nutraceuticals. As a result, *C. cristata* extracts can be evaluated as a natural agent that provides multifaceted protection against UV-induced oxidative stress, DNA damage, cell proliferation, and ECM degradation. These findings have shown that the extracts obtained from *C. cristata* have the potential to be transformed into antiaging products, other products used in the cosmetic industry, and pharmaceutical products, thanks to their high antioxidants and phytoconstituent diversity.

4 | Experimental

4.1 | Plant Collection

In 2023, a botanical sample collection was carried out in Muğla, Turkey (C2 Muğla: Muğla-Bodrum road, 25 km from Muğla, roadside, 37°12′0.64″ N, 27°37′44.38″ E, 136 m). The taxonomic identification of the collected specimens was meticulously carried out by Dr. Selami Selvi, a specialist in botany. A voucher specimen was formally deposited in the herbarium of Balıkesir University (voucher number: SV 3859) for future reference and verification. After collecting, the aerial parts of the plant were carefully separated and subjected to shade drying at ambient temperature to preserve their phytochemical integrity. The dried material was then finely ground into powder using a standardized process. To prevent

degradation and ensure long-term stability, the powdered plant material was stored in light-proof containers under controlled conditions.

4.2 | Plant Extract Preparation

The extraction method employed four distinct solvents: ethyl acetate, ethanol, a 70% ethanol/water mixture, and water. A 10-gram sample was macerated with 200 mL of ethyl acetate, ethanol, and an ethanol–water mixture for a duration of 24 h at ambient temperature. The aqueous extract was obtained by infusing 10 g of plant material in boiling water for a period of 15 min. Subsequent to this, the organic solvents were eliminated through evaporation under low pressure, and the aqueous extract was then subjected to freeze-drying.

4.3 | Assay for Total Phenolic and Flavonoid Contents

Total phenolics and flavonoids were quantified in our previous paper [126]. Folin-Ciocalteu and $AlCl_3$ assays were performed for quantifying these components, respectively. GA and rutin (R) served as reference standards in the experiments, with results reported as gallic acid equivalents (GAE) and rutin equivalents (RE).

4.4 | LC-ESI-QTOF-MS Analysis

Chromatographic analysis was conducted using an Agilent 6550 QTOF LC/MS (Agilent, Santa Clara, CA, USA) equipped with an electrospray ionization source (ESI) to identify and characterize polyphenols in the extracts. Separation was achieved with an Agilent Poroshell 120 SB-C18 column (3.0 × 100 mm, 2.7 μm particle size). All experimental details are described in our earlier paper [127].

4.5 | Assays for In Vitro Antioxidant Capacity

As previously described [128], Trolox equivalents (TE) per gram were calculated for radical scavenging with FRAP, CUPRAC, DPPH, and ABTS. The antioxidant potential was determined in millimoles of TE per gram of extract using the phosphomolybdenum (PBD) assay, and the metal chelating activity (MCA) was quantified in EDTAE.

4.6 | Inhibitory Effects Against Some Key Enzymes

Enzyme inhibition studies were performed on samples according to methods [128]. Galanthamine equivalents (GALAE) in milligrams were employed to assess the inhibition of AChE and BChE. In contrast, acarbose equivalents (ACAE) per gram of extract served as the unit for assessing amylase and glucosidase inhibition. The inhibition of tyrosinase was quantified using milligrams of kojic acid equivalents per gram of extract.

4.7 | Detection of AGEs Inhibition

The BSA-glycation model, which was previously optimized by us, was used to determine the effect of four different extracts obtained from the Cachrys cristata plant (ethyl acetate, ethanol, ethanol/water (70%), and water (infused) on the inhibition of advanced glycation products (AGEs) at a concentration of 1 mg/mL [48, 129]. First, the samples at 1 mg/mL were taken into separate tubes, mixed with 1 mg/L bovine serum albumin (BSA) prepared in 0.1 M phosphate buffered saline (PBS) and 0.5 M glucose, and incubated in the dark at 37°C for 2 days. While the test groups contained the extracts, the group containing only BSA and glucose was used as a positive control and the group containing only BSA was used as a negative control. In the experimental setup where Quercetin was used as a positive control at increasing concentrations (62.5 μg/mL–1000 μg/mL), incubation probe analyses were performed by measuring fluorescence (Ex: 370 nm, Em: 440 nm) [48, 129].

4.8 | Cell Culture

HDF cells were cultured in complete Dulbecco's Modified Eagle Medium (DMEM) enriched with 10% fetal bovine serum (FBS), 1% Penicillin-Streptomycin (100 U/mL Penicillin, 100 μg/mL Streptomycin), and 1% L-Glutamine. After reaching approximately 85% confluency in the growth plates, HDFs were passaged with 0.25% Trypsin-EDTA solution and substocks were banked in liquid nitrogen [68, 129]. In addition, to obtain UV-induced HDF cells that will form the experimental group in further in vitro studies, UVB irradiation was applied to 1×10^6 HDF with a UVB cross-linker at a power of 0.5 J/cm² for 3 min [80].

4.9 | Determination of Nontoxic Concentration of *C. cristata* by WST-1

To determine the nontoxic concentration of four different extracts obtained from Cachrys cristata (ethyl acetate, ethanol, ethanol/water (70%), and water (infused)), HDF cells were seeded in 96-well plates at a number of 10,000 cells/well and incubated for 16 h for the cells to adhere to the wells. At the end of incubation, cells were treated with four different extracts at increasing concentrations (50–250 μg/mL) at 37°C in a 5% CO_2 and 95% O_2 environment for 48 h. After 48 h, 10 μL of WST-1 reagent and 90 μL of DMEM were mixed at a ratio of 1:10 and added to the cells washed with 1X phosphate buffer saline (PBS). Cells incubated with WST-1 reagent for 45 min were measured for absorbance at a wavelength of 570 nm to determine nontoxic concentration and cell proliferation [68, 129].

4.10 | Determination of Cellular Antioxidant Levels With DCFDA

Following the application of ethyl acetate, ethanol, ethanol/water (70%), and WEs obtained from *C. cristata* to UV-induced HDF cells, the changing mitochondrial reactive oxygen levels were determined by DCFDA assay [68, 129]. Nontreated HDF cells defined as the control group were not treated with UV and

extracts obtained from *C. cristata*, while the sample groups consisted of UV-induced HDF and UV-induced HDF cells to which extracts obtained from *C. cristata* were applied. UV-induced HDF cells to which EGCG was applied were used as a positive control [68, 129].

4.11 | Comet Assay

HDF cells (5×10^4 cells/well) were seeded in 6-well plates and incubated for 24 h, then exposed to 0.5 J/cm² UV exposure and then treated with 150 μg/mL extracts for 48 h. Cells were washed with PBS (pH 7.4), collected with 0.05% Trypsin-EDTA, and centrifuged at 1000 rpm for 5 min, then the pellet was suspended in cold PBS. Suspended cells were counted, 200 cells were mixed with 1% low-soluble agarose and spread on the slide and left for 1 h. Then, 0.5% normal agarose was spread on the slide and left for 60 min at 4°C to cover it. Following the incubation period, the slides were incubated in lysis buffer (2.5 M NaCl, 100 mM EDTA, 10 mM Tris, 1% Triton X-100, pH 10) for 1 h at 4°C. In the next step, the slides were kept in alkaline electrophoresis buffer (300 mM NaOH, 1 mM EDTA, pH > 13) for 20 min. Then, electrophoresis was applied at 25 V, 300 mA for 20 min in a cold room and in the dark. After the slides were transferred to the neutralization solution, they were stained with 1 μg/mL DAPI, and DNA damage was evaluated under a fluorescence microscope. DNA tail length and percentage were analyzed with CaspLab software [80, 130].

4.12 | Determination of Protein Levels in the Molecular Pathway by Western Blot

The effects of ethyl acetate, ethanol, ethanol/water (70%), and WEs obtained from *C. cristata* applied to UV-induced HDF cells on protein synthesis were determined by the Western Blot method. After incubating UV-induced HDFs with model plant extracts for 48 h, the Bradford assay was applied to collect the protein content in the cells, and 30 μg of total protein was taken for each sample and separated on a 12% SDS-PAGE gel. After the proteins were transferred to PVDF membrane, they were incubated with primary antibodies (p-NFκB p65, AP-1, RAGE, β-actin; 1:5000 dilution) at 4°C overnight. The next day, the membranes were washed with TBS-T buffer and incubated with HRP-conjugated secondary antibody (1:5000) at room temperature for 1 h. After the incubation step, protein levels were detected with the ChemiDoc imaging system using ECL. β-actin was used to prove that equal amounts of protein sample were loaded into all wells, and band thicknesses were normalized with ImageJ software by comparing to β-actin [48, 61].

4.13 | Gelatin Zymography

Following UV induction of HDF cells, changes in the ECM composition were measured by gelatin zymography technique after application of four different extracts obtained from *C. cristata*. To observe changes in the biosynthesis of MMP-2 and MMP-9, which are ECM components, the growth medium of the cells was collected and loaded onto a 10% SDS-free polyacrylamide gel containing 1% gelatin substrate, and the gel was electrophoresed in cold running buffer for 2 h. To make the lytic transparent bands visible in the gel, the gels were stained with Coomassie Brilliant Blue R-250, and the intensity of the white bands was quantitatively analyzed using ImageJ software depending on the MMP-2 and MMP-9 enzyme activity [61, 129, 131].

4.14 | Inhibitory Activity of Enzymes Involved in the Destruction of Skin Tissue

Anticollagenase, antielastase, and antihyaluronidase tests were performed to reveal the potential of four different extracts obtained from *C. cristata* in breaking down the skin barrier and inhibiting enzymes that cause aging. In this context, 50 mM Tris–HCl buffer (pH 7.4) was used for collagenase, 200 mM Tris–HCl buffer (pH 8.0) for elastase, and 0.1 M acetate buffer (pH 4.5) for hyaluronidase, respectively [132]. Then, the extracts were incubated with the prepared enzyme/substrate mixture and the inhibitory potential of *C. cristata* was measured by taking absorbance at 340 nm for collagenase, 410 nm for elastase, and 600 nm for hyaluronidase, respectively [132]. In the experimental setup, EGCG at a concentration of 250 μg/mL was used as a positive control for anticollagenase and antielastase, while tannic acid at a concentration of 250 μg/mL was used as a positive control for the antihyaluronidase test [133].

4.15 | Network Pharmacology

The network pharmacology study commenced with the identification of molecular targets for the selected compounds via the Comparative Toxicogenomics Database (CTD) and PubChem databases. The aforementioned targets were employed to construct a protein–protein interaction (PPI) network, which was subsequently visualized using Cytoscape V3.10.2 software [134, 135]. During the network analysis, nodes with a degree value of 2 or higher were identified as key genes, and these genes were validated using the STRING plugin in Cytoscape. Subsequently, these genes were employed once more to construct a PPI network in the STRING v12.0 database. The analyses were conducted with a confidence score threshold of ≥ 0.4, selecting "Homo sapiens" as the species of interest [136]. High-degree nodes were subjected to Disease Ontology (DO) enrichment analysis using the DOSE package (V3.30.1) in R to identify their associations with relevant disease processes [137]. Additionally, KEGG pathway enrichment analysis was conducted using the DAVID database to explore the biological pathways involving these proteins.

4.16 | Molecular Docking

Molecular docking was performed to gain insights into the binding mode and interaction pattern of the bioactive compounds in the extract of the aerial parts of *C. cristata*. All available protein 3D structures were retrieved from the protein databank with the following IDs: human AChE (PDB ID: 7E3H) [138], BChE (PDB ID: 7Q3Q) [139], and α-amylase (PDB ID: 1B2Y) [122]. Furthermore, the homology models of human tyrosinase and glucosidase enzymes were also retrieved from a previous study [140]. The structures were prepared by optimizing H bonds using the Epik,

Prime module of Maestro 2019-2 (Schrodinger LLC, New York), adjusting bond orders, adding hydrogen atoms and missing heavy atoms, assigning partial charges, and protonation state to titratable residues. Glide extra-precision (XP) scoring function was used to dock each ligand into the selected proteins (2019-2, Schrodinger LLC, New York) utilizing the cocrystal ligand-binding site grids generated by Maestro's receptor grid panel [141]. Similarly, all ligand 3D structures were downloaded from the PubChem database (https://pubchem.ncbi.nlm.nih.gov/) and prepared using the LigPrep module of Maestro (2019-2, Schrodinger LLC, New York), employing the conjugate gradient algorithm. Finally, Maestro Viewer was used to generate 2D protein–ligand interaction diagrams.

4.17 | Calculation of MM/PBSA Free Energy to Determine Ligand-Binding Affinity

The study employed the gmx_MMPBSA tool (https://valdes-tresanco-ms.github.io/gmx_MMPBSA/dev/getting-started/) to evaluate the stability and calculate the binding free energy of various molecular complexes. To evaluate the stability of the aforementioned complexes, 10-ns MD simulations were conducted. The complexes Quercetin_MMP9, Rutin_AChE, Rutin_BChE, Rutin_Collagenase, Rutin_Hyaluronidase, and Rutin_MMP2 were subjected to MD simulations. Based on these simulations, the complexes demonstrating the highest stability were identified and selected for further investigation. These selected complexes were then subjected to extended 100-ns MD simulations to gain deeper insights into their interactions and potential as therapeutic candidates [142, 143].

4.18 | MD Simulation Setup for Ligand Stability and Flexibility

MD simulations were conducted utilizing the CHARMM graphical user interface (GUI) platform (https://charmm-gui.org). The system configuration was performed using the Solution Builder tool, as previously described by Jo et al. [144]. The CHARMM36m force field was employed for protein parameterization, in accordance with the methodologies delineated by Yagi et al. [145] and Maier et al. [146]. A periodic boundary box with TIP3P water molecules was utilized, thereby ensuring a minimum separation of 10 Å between the protein and the box boundaries. Counterions were introduced to achieve electroneutrality and to adjust the concentration of NaCl to 0.15 M. The Verlet cutoff scheme was employed to manage electrostatic and van der Waals interactions, while the LINCS algorithm was utilized to constrain bond lengths. The long-range electrostatics were calculated using the particle mesh Ewald (PME) method. The system was then subjected to energy minimization using the steepest descent algorithm, with the objective of reducing the potential energy variation to a value of less than 1000 kJ/mol/nm. The system was equilibrated under both NVT and NPT conditions at 303.3 K, ensuring thermodynamic stability. Subsequently, production simulations for a total of 100 ns (nstep = 50,000,000) were performed using GROMACS 2023.2. These simulations were conducted for the Quercetin_MMP-9, Rutin_MMP-2, and Rutin_BChE complexes to investigate their stability, interactions, and potential as therapeutic candidates.

4.19 | Statistical Analysis

GraphPad 8.1 software was used for quantitative analysis of all experiments presented within the scope of in vitro studies. Experiments were evaluated independently and at different times by repeating them at least three times.

Conflicts of Interest

The authors declare no conflicts of interest.

Data Availability Statement

The data that support the findings of this study are available from the corresponding author upon reasonable request.

References

1. E. Tvrdá and F. Benko, "Free Radicals: What They Are and What They do," *Pathology* (Elsevier, 2020), 3–13.

2. S. Nilofar, S. Dall'Acqua, S. Sut, et al., "Exploring the Effects of Post-Distillation and Post-Supercritical CO2 Extraction on Chemical Profile and Biological Activities of Two Salvia Species (S. *chrysophylla* and *S. microstegia*)," *Microchemical Journal* 198 (2024): 110183.

3. A. Junsongduang, W. Kasemwan, S. Lumjoomjung, W. Sabprachai, W. Tanming, and H. Balslev, "Ethnomedicinal Knowledge of Traditional Healers in Roi Et, Thailand," *Plants* 9, no. 9 (2020): 1177.

4. R. Makhuvele, K. Naidu, S. Gbashi, V. C. Thipe, O. A. Adebo, and P. B. Njobeh, "The Use of Plant Extracts and Their Phytochemicals for Control of Toxigenic Fungi and Mycotoxins," *Heliyon* 6, no. 10 (2020): e05291.

5. A. M. Alamgeer, A. M. Uttra, H. Ahsan, U. H. Hasan, and M. A. Chaudhary, "Traditional Medicines of Plant Origin Used for the Treatment of Inflammatory Disorders in Pakistan: A Review," *Journal of Traditional Chinese Medicine* 38, no. 4 (2018): 636–656.

6. Z. Zhao, Y. Li, L. Zhou, et al., "Prevention and Treatment of COVID-19 Using Traditional Chinese Medicine: A Review," *Phytomedicine* 85 (2021): 153308.

7. S. Tesfaye, K. Asres, E. Lulekal, et al., "Ethiopian Medicinal Plants Traditionally Used for the Treatment of Cancer, Part 2: A Review on Cytotoxic, Antiproliferative, and Antitumor Phytochemicals, and Future Perspective," *Molecules* 25, no. 17 (2020): 4032.

8. A. Alesci, M. Aragona, N. Cicero, and E. R. Lauriano, "Can Nutraceuticals Assist Treatment and Improve Covid-19 Symptoms?," *Natural Product Research* 36, no. 10 (2022): 2672–2691.

9. B. Salehi, P. Zucca, M. Sharifi-Rad, et al., "Phytotherapeutics in Cancer Invasion and Metastasis," *Phytotherapy Research* 32, no. 8 (2018): 1425–1449.

10. P. J. Houghton, "Old yet New—Pharmaceuticals From Plants," *Journal of Chemical Education* 78, no. 2 (2001): 175.

11. G. Cravotto, L. Boffa, L. Genzini, and D. Garella, "Phytotherapeutics: An Evaluation of the Potential of 1000 Plants," *Journal of Clinical Pharmacy and Therapeutics* 35, no. 1 (2010): 11–48.

12. S. M. Musthaba, S. Baboota, S. Ahmed, A. Ahuja, and J. Ali, "Status of Novel Drug Delivery Technology for Phytotherapeutics," *Expert Opinion on Drug Delivery* 6, no. 6 (2009): 625–637.

13. V. Dave, R. B. Yadav, R. Ahuja, and S. Yadav, "Formulation Design and Optimization of Novel Fast Dissolving Tablet of Chlorpheniramine Maleate by Using Lyophilization Techniques," *Bulletin of Faculty of Pharmacy, Cairo University* 55, no. 1 (2017): 31–39.

14. G. M. Cragg and D. J. Newman, "Natural Products: A Continuing Source of Novel Drug Leads," *Biochimica et Biophysica Acta (BBA)-General Subjects* 1830, no. 6 (2013): 3670–3695.

15. P. P. Ferrer-Gallego and J. F. Alos, "(2822) Proposal to Conserve the Name Cachrys Libanotis (Umbelliferae) With a Conserved Type," *Taxon* 70, no. 3 (2021): 682–684.

16. V. Musolino, M. R. Perri, F. Conforti, M. Gliozzi, M. Marrelli, and V. Mollace, "Cachrys L. Genus: A Comprehensive Review on Botany, Phytochemistry and Biological Properties," *Plants* 12, no. 3 (2023): 565.

17. M. Grande, M. T. Aguado, B. Mancheño, and F. Piera, "Coumarins and Ferulol Esters From Cachrys Sicula," *Phytochemistry* 25, no. 2 (1986): 505–507.

18. M. A. Khalilzadeh, M. Tajbakhsh, F. A. Gholami, et al., "Composition of the Essential Oils of Hippomarathrum Microcarpum (M. Bieb.) B. Fedtsch. and Physospermum Cornubiense (L.) DC. From Iran," *Journal of Essential Oil Research* 19, no. 6 (2007): 567–568.

19. M. Marrelli, M. R. Perri, V. Amodeo, et al., "Assessment of Photo-Induced Cytotoxic Activity of Cachrys Sicula and Cachrys Libanotis Enriched-Coumarin Extracts Against Human Melanoma Cells," *Plants* 10, no. 1 (2021): 123.

20. G. Menichini, C. Alfano, E. Provenzano, et al., "Cachrys Pungens Jan Inhibits Human Melanoma Cell Proliferation Through Photo-Induced Cytotoxic Activity," *Cell Proliferation* 45, no. 1 (2012): 39–47.

21. M. R. Perri, M. Pellegrino, S. Aquaro, et al., "Cachrys spp. From Southern Italy: Phytochemical Characterization and JAK/STAT Signaling Pathway Inhibition," *Plants* 11, no. 21 (2022): 2913.

22. T. Özek, G. Özek, and S. Yur, "Phytochemical and Biological Characteristics of Apiaceae Species From Turkey, *Medicinal and Aromatic Plants of Turkey*, eds. Á. Máthé and K. Turgut (Springer, 2023), 73–106.

23. Tutin, T. G., "*Flora Europaea 2*," in Genus Cachrys, eds. T. G. Tutin, V. H. Heywood, N. A. Burges et al. (Cambridge University Press, 1968), 343.

24. G. Özek, T. Özek, K. H. C. Başer, E. Hamzaoglu, and A. Duran, "Composition of the Essential Oil of Hippomarathrum Cristatum (DC.) Boiss," *Journal of Essential Oil Research* 19, no. 6 (2007): 540–542.

25. S. Aryal, M. K. Baniya, K. Danekhu, P. Kunwar, R. Gurung, and N. Koirala, "Total Phenolic Content, Flavonoid Content and Antioxidant Potential of Wild Vegetables From Western Nepal," *Plants* 8, no. 4 (2019): 96.

26. R. E. Barrientos, S. Ahmed, C. Cortés, et al., "Chemical Fingerprinting and Biological Evaluation of the Endemic Chilean Fruit Greigia Sphacelata (Ruiz and Pav.) Regel (Bromeliaceae) by UHPLC-PDA-Orbitrap-Mass Spectrometry," *Molecules* 25, no. 16 (2020): 3750.

27. J. S. Matejic, A. M. Dzamic, T. M. Mihajilov-Krstev, V. N. Randjelovic, K. S. Mileski, and P. D. Marin, "Total Phenolic and Flavonoid Contents and Biological Activities of Cachrys Cristata Dc. Extracts," *Archives of Biological Sciences* 66, no. 3 (2014): 1117–1123.

28. F. Araniti, M. Marrelli, A. Lupini, F. Mercati, G. A. Statti, and M. R. Abenavoli, "Phytotoxic Activity of Cachrys Pungens Jan, a Mediterranean Species: Separation, Identification and Quantification of Potential Allelochemicals," *Acta Physiologiae Plantarum* 36 (2014): 1071–1083.

29. O. Tusevski, A. Kostovska, A. Iloska, L. Trajkovska, and S. G. Simic, "Phenolic Production and Antioxidant Properties of Some Macedonian Medicinal Plants," *Central European Journal of Biology* 9 (2014): 888–900.

30. G. Cao and R. L. Prior, "Comparison of Different Analytical Methods for Assessing Total Antioxidant Capacity of Human Serum," *Clinical Chemistry* 44, no. 6 (1998): 1309–1315.

31. M. Asif, "Chemistry and Antioxidant Activity of Plants Containing Some Phenolic Compounds," *Chemistry International* 1, no. 1 (2015): 35–52.

32. N. Shen, T. Wang, Q. Gan, S. Liu, L. Wang, and B. Jin, "Plant Flavonoids: Classification, Distribution, Biosynthesis, and Antioxidant Activity," *Food Chemistry* 383 (2022): 132531.

33. İ. Gulcin, "Antioxidants and Antioxidant Methods: An Updated Overview," *Archives of Toxicology* 94, no. 3 (2020): 651–715.

34. Y. Wang, Y. Su, Q. Shehzad, et al., "Comparative Study on Quality Characteristics of Bischofia Polycarpa Seed Oil by Different Solvents: Lipid Composition, Phytochemicals, and Antioxidant Activity," *Food Chemistry: X* 17 (2023): 100588.

35. K. I. Nilofar, K. I. Sinan, O. E. Eyupoglu, et al., "Multiple Online-HPLC Methodologies and Biological Properties of Leaves and Stem Barks Extracts of Chrysanthellum Indicum," *Microchemical Journal* 197 (2024): 109847.

36. S. Bhadra, C. Pundir, J. Das, et al., "Evaluation of Bioactive Compounds as AChE Inhibitors From Medicinal Plants," in *Evidence-Based Validation of Herbal Medicine*, ed. P. K. Mukherjee (Elsevier, 2022), 349–388.

37. M. B. Colovic, D. Z. Krstic, T. D. Lazarevic-Pasti, A. M. Bondzic, and V. M. Vasic, "Acetylcholinesterase Inhibitors: Pharmacology and Toxicology," *Current Neuropharmacology* 11, no. 3 (2013): 315–335.

38. Z. Y. Ha, S. Mathew, and K. Y. Yeong, "Butyrylcholinesterase: A Multifaceted Pharmacological Target and Tool," *Current Protein & Peptide Science* 21, no. 1 (2020): 99–109.

39. G. Marucci, M. Buccioni, D. D. Ben, C. Lambertucci, R. Volpini, and F. Amenta, "Efficacy of Acetylcholinesterase Inhibitors in Alzheimer's Disease," *Neuropharmacology* 190 (2021): 108352.

40. S. Tahar, B. Hamdi, G. Flamini, et al., "Chemical Composition, Antioxidant and Anticholinesterase Activity of the Essential Oil of Algerian Cachrys Sicula L," *Natural Product Research* 36, no. 16 (2022): 4094–4102.

41. G. Albayrak, S. Demir, K. Halil, and S. Baykan, "Anticholinesterase and Antityrosinase Activities of Endemic Prangos Heyniae H. Duman & MF Watson and Its Metabolites," *İstanbul Journal of Pharmacy* 53, no. 1 (2023): 51–57.

42. I. Nilofar, T. Duran, A. I. Uba, et al., "Extractions of Aerial Parts of Hippomarathrum Scabrum With Conventional and Green Methodologies: Chemical Profiling, Antioxidant, Enzyme Inhibition, and Anti-Cancer Effects," *Journal of Separation Science* 47, no. 1 (2024): 2300678.

43. S. Zahra, S. Zaib, and I. Khan, "Identification of Isobenzofuranone Derivatives as Promising Antidiabetic Agents: Synthesis, In Vitro and In Vivo Inhibition of α-Glucosidase and α-Amylase, Computational Docking Analysis and Molecular Dynamics Simulations," *International Journal of Biological Macromolecules* 259 (2024): 129241.

44. H. Rasouli, S. M. Hosseini-Ghazvini, H. Adibi, and R. Khodarahmi, "Differential α-Amylase/α-Glucosidase Inhibitory Activities of Plant-Derived Phenolic Compounds: A Virtual Screening Perspective for the Treatment of Obesity and Diabetes," *Food & Function* 8, no. 5 (2017): 1942–1954.

45. Y. S. Hamed, M. Abdin, A. M. Rayan, H. M. Saleem Akhtar, and X. Zeng, "Synergistic Inhibition of Isolated Flavonoids From *Moringa oleifera* Leaf on α-Glucosidase Activity," *Lwt* 141 (2021): 111081.

46. K. Zhang, Z. Ding, W. Duan, et al., "Optimized Preparation Process for Naringenin and Evaluation of Its Antioxidant and α-Glucosidase Inhibitory Activities," *Journal of Food Processing and Preservation* 44, no. 12 (2020): e14931.

47. A. B. Uceda, L. Mariño, R. Casasnovas, and M. Adrover, "An Overview on Glycation: Molecular Mechanisms, Impact on Proteins, Pathogenesis, and Inhibition," *Biophysical Reviews* 16, no. 2 (2024): 189–218, https://doi.org/10.1007/s12551-024-01188-4.

48. T. H. Barak, İ. Kurt-Celep, and E. Celep, "Bioaccessibility and Functional Food Potential of *Equisetum telmateia* Ehrh. Against Diabetes-Induced Kidney Disorders," *Foods* 13, no. 24 (2024): 4092.

49. K. Zgutka, M. Tkacz, P. Tomasiak, and M. Tarnowski, "A Role for Advanced Glycation End Products in Molecular Ageing," *International Journal of Molecular Sciences* 24, no. 12 (2023): 9881.

50. K. Jomova, R. Raptova, S. Y. Alomar, et al., "Reactive Oxygen Species, Toxicity, Oxidative Stress, and Antioxidants: Chronic Diseases and Aging," *Archives of Toxicology* 97, no. 10 (2023): 2499–2574, https://doi.org/10.1007/s00204-023-03562-9.

51. V. Cepas, M. Collino, J. C. Mayo, and R. M. Sainz, "Redox Signaling and Advanced Glycation Endproducts (AGEs) in Diet-Related Diseases," *Antioxidants* 9, no. 2 (2020): 142.

52. Y. Chen, Z. Meng, Y. Li, S. Liu, P. Hu, and E. Luo, "Advanced Glycation End Products and Reactive Oxygen Species: Uncovering the Potential Role of Ferroptosis in Diabetic Complications," *Molecular Medicine* 30, no. 1 (2024): 141, https://doi.org/10.1186/s10020-024-00905-9.

53. M. Maisto and G. C. Tenore, "Polyphenols as a Useful Tool to Ameliorate Advanced Glycation End-Product Formation: A Focus on Molecular Mechanisms of Action," *Frontiers in Bioscience-Landmark* 29, no. 12 (2024): 424, https://doi.org/10.31083/j.fbl2912424.

54. C.-H. Wu, S.-M. Huang, J.-A. Lin, and G.-C. Yen, "Inhibition of Advanced Glycation Endproduct Formation by Foodstuffs," *Food & Function* 2, no. 5 (2011): 224–234, https://doi.org/10.1039/C1FO10026B.

55. D. de Paulo Farias, F. F. de Araújo, I. A. Neri-Numa, and G. M. Pastore, "Antidiabetic Potential of Dietary Polyphenols: A Mechanistic Review," *Food Research International* 145 (2021): 110383, https://doi.org/10.1016/j.foodres.2021.110383.

56. M. Martiniakova, A. Sarocka, N. Penzes, et al., "Protective Role of Dietary Polyphenols in the Management and Treatment of Type 2 Diabetes Mellitus," *Nutrients* 17, no. 2 (2025): 275.

57. C.-H. Wu and G.-C. Yen, "Inhibitory Effect of Naturally Occurring Flavonoids on the Formation of Advanced Glycation Endproducts," *Journal of Agricultural and Food Chemistry* 53, no. 8 (2005): 3167–3173, https://doi.org/10.1021/jf048550u.

58. L. Zeng, H. Ding, X. Hu, G. Zhang, and D. Gong, "Galangin Inhibits α-Glucosidase Activity and Formation of Non-Enzymatic Glycation Products," *Food Chemistry* 271 (2019): 70–79, https://doi.org/10.1016/j.foodchem.2018.07.148.

59. S. P. Ekambaram, S. S. Perumal, and S. Paramasivam, "Galangin: Advances on Resources, Biosynthesis Pathway, Bioavailability, Bioactivity, and Pharmacology," in *Handbook of Dietary Flavonoids*, eds. J. Xiao (Springer International Publishing, 2023), 1–59.

60. F. Zhang, Y. Yan, L.-M. Zhang, et al., "Pharmacological Activities and Therapeutic Potential of Galangin, a Promising Natural Flavone, in Age-Related Diseases," *Phytomedicine* 120 (2023): 155061, https://doi.org/10.1016/j.phymed.2023.155061.

61. I. Kurt-Celep, S. Yagi, S. Dall'Acqua, et al., "From Parasitic Life to Health-Promoting Applications—A Versatile Goldmine Discovered in Nature's Secret Treasure Chest: Orobanche Nana," *Food Bioscience* 62 (2024): 105296, https://doi.org/10.1016/j.fbio.2024.105296.

62. E. Scarcello, A. Lambremont, R. Vanbever, P. J. Jacques, and D. Lison, "Mind Your Assays: Misleading Cytotoxicity With the WST-1 Assay in the Presence of Manganese," *PLoS One* 15, no. 4 (2020): e0231634, https://doi.org/10.1371/journal.pone.0231634.

63. E. Nissen, G. Pauli, and D. Vollenbroich, "WST-1 Assay—A Simple Colorimetric Method for Virus Titration," *In Vitro Cellular & Developmental Biology- Animal* 33, no. 1 (1997): 28–29, https://doi.org/10.1007/s11626-997-0018-1.

64. D. Stan, A.-M. Enciu, A. L. Mateescu, et al., "Natural Compounds With Antimicrobial and Antiviral Effect and Nanocarriers Used for Their Transportation," *Frontiers in Pharmacology* 12 (2021): 723233, https://doi.org/10.3389/fphar.2021.723233.

65. E. Brglez Mojzer, M. Knez Hrnčič, M. Škerget, Ž. Knez, and U. Bren, "Polyphenols: Extraction Methods, Antioxidative Action, Bioavailability and Anticarcinogenic Effects," *Molecules* 21, no. 7 (2016): 901.

66. S. Ahmed, G. Zengin, Á. Fernández-Ochoa, et al., "Exploration of UHPLC-ESI-QTOF-MS Profiles and the Neuroprotective, Antidiabetic, Antioxidant and Cytotoxic Effects of Extracts From Achillea Maritima (L.) Ehrend.And Y.P.Guo (Asteraceae) Collected in Türkiye," *Plant Foods for Human Nutrition (Dordrecht, Netherlands)* 80, no. 1 (2025): 66, https://doi.org/10.1007/s11130-025-01314-x.

67. İ. Kurt-Celep, G. Zengin, A. I. Uba, et al., "Unraveling the Chemical Profile, Antioxidant, Enzyme Inhibitory, Cytotoxic Potential of Different Extracts From *Astragalus caraganae*," *Archiv der Pharmazie* 356, no. 9 (2023): e2300263, https://doi.org/10.1002/ardp.202300263.

68. I. Kurt-Celep, D. Zheleva-Dimitrova, K. I. Sinan, et al., "Uncovering Chemical Profiles, Biological Potentials, and Protection Effect Against ECM Destruction in H2O2-Treated HDF Cells of the Extracts of Stachys Tundjeliensis," *Archiv der Pharmazie* 357, no. 2 (2024): 2300528, https://doi.org/10.1002/ardp.202300528.

69. M. Wei, X. He, N. Liu, and H. Deng, "Role of Reactive Oxygen Species in Ultraviolet-Induced Photodamage of the Skin," *Cell Division* 19, no. 1 (2024): 1, https://doi.org/10.1186/s13008-024-00107-z.

70. G. Martemucci, C. Costagliola, M. Mariano, L. D'andrea, P. Napolitano, and A. G. D'Alessandro, "Free Radical Properties, Source and Targets, Antioxidant Consumption and Health," *Oxygen* 2, no. 2 (2022): 48–78.

71. A. Intharuksa, S. Kuljarusnont, Y. Sasaki, and D. Tungmunnithum, "Flavonoids and Other Polyphenols: Bioactive Molecules From Traditional Medicine Recipes/Medicinal Plants and Their Potential for Phytopharmaceutical and Medical Application," *Molecules* 29, no. 23 (2024): 5760.

72. S. C. Lourenço, M. Moldão-Martins, and V. D. Alves, "Antioxidants of Natural Plant Origins: From Sources to Food Industry Applications," *Molecules* 24, no. 22 (2019): 4132.

73. M. Zahra, H. Abrahamse, and B. P. George, "Flavonoids: Antioxidant Powerhouses and Their Role in Nanomedicine," *Antioxidants* 13, no. 8 (2024): 922.

74. P. Sitarek, A. Merecz-Sadowska, J. Sikora, et al., "Flavonoids and Their Derivatives as DNA Topoisomerase Inhibitors With Anti-Cancer Activity in Various Cell Models: Exploring a Novel Mode of Action," *Pharmacological Research* 209 (2024): 107457, https://doi.org/10.1016/j.phrs.2024.107457.

75. X. Xi, J. Wang, Y. Qin, Y. You, W. Huang, and J. Zhan, "The Biphasic Effect of Flavonoids on Oxidative Stress and Cell Proliferation in Breast Cancer Cells," *Antioxidants* 11, no. 4 (2022): 622.

76. I. Kostova, S. Bhatia, P. Grigorov, et al., "Coumarins as Antioxidants," *Current Medicinal Chemistry* 18, no. 25 (2011): 3929–3951, https://doi.org/10.2174/092986711803414395.

77. W.-B. Li, X.-P. Qiao, Z.-X. Wang, S. Wang, and S.-W. Chen, "Synthesis and Antioxidant Activity of Conjugates of Hydroxytyrosol and Coumarin," *Bioorganic Chemistry* 105 (2020): 104427, https://doi.org/10.1016/j.bioorg.2020.104427.

78. J. Atkinson, E. Bezak, H. Le, and I. Kempson, "DNA Double Strand Break and Response Fluorescent Assays: Choices and Interpretation," *International Journal of Molecular Sciences* 25, no. 4 (2024): 2227.

79. J. M. Danforth, L. Provencher, and A. A. Goodarzi, "Chromatin and the Cellular Response to Particle Radiation-Induced Oxidative and Clustered DNA Damage," *Frontiers in Cell and Developmental Biology* 10 (2022): 910440, https://doi.org/10.3389/fcell.2022.910440.

80. İ. Kurt-Celep, E. Celep, S. Akyüz, et al., "Hypericum Olympicum L. Recovers DNA Damage and Prevents MMP–9 Activation Induced by UVB in Human Dermal Fibroblasts," *Journal of Ethnopharmacology* 246 (2020): 112202, https://doi.org/10.1016/j.jep.2019.112202.

81. G. Borges Bubols, D. da Rocha Vianna, A. Medina-Remon, et al., "The Antioxidant Activity of Coumarins and Flavonoids," *Mini-Reviews in Medicinal Chemistry* 13, no. 3 (2013): 318–334.

82. M. Grazul and E. Budzisz, "Biological Activity of Metal Ions Complexes of Chromones, Coumarins and Flavones," *Coordination*

Chemistry Reviews 253, no. 21 (2009): 2588–2598, https://doi.org/10.1016/j.ccr.2009.06.015.

83. T. L. de Jager, A. E. Cockrell, and S. S. Du Plessis, "Ultraviolet Light Induced Generation of Reactive Oxygen Species," in *Ultraviolet Light in Human Health, Diseases and Environment*, eds. S. I. Ahmad (Springer International Publishing, 2017), 15–23.

84. S. Shadfar, S. Parakh, M. S. Jamali, and J. D. Atkin, "Redox Dysregulation as a Driver for DNA Damage and Its Relationship to Neurodegenerative Diseases," *Translational Neurodegeneration* 12, no. 1 (2023): 18, https://doi.org/10.1186/s40035-023-00350-4.

85. C. A. Juan, J. M. Pérez de la Lastra, F. J. Plou, and E. Pérez-Lebeña, "The Chemistry of Reactive Oxygen Species (ROS) Revisited: Outlining Their Role in Biological Macromolecules (DNA, Lipids and Proteins) and Induced Pathologies," *International Journal of Molecular Sciences* 22, no. 9 (2021): 4642.

86. S. Alsawaf, F. Alnuaimi, S. Afzal, et al., "Plant Flavonoids on Oxidative Stress-Mediated Kidney Inflammation," *Biology* 11, no. 12 (2022): 1717.

87. S. Quraishi, D. Saha, K. Kumari, A. N. Jha, and A. S. Roy, "Non-Covalent Binding Interaction of Bioactive Coumarin Esculetin With Calf Thymus DNA and Yeast Transfer RNA: A Detailed Investigation to Decipher the Binding Affinities, Binding Location, Interacting Forces and Structural Alterations at a Molecular Level," *International Journal of Biological Macromolecules* 257 (2024): 128568, https://doi.org/10.1016/j.ijbiomac.2023.128568.

88. P. Kowalczyk, A. Madej, D. Paprocki, M. Szymczak, and R. Ostaszewski, "Coumarin Derivatives as New Toxic Compounds to Selected K12, R1–R4 *E. coli* Strains," *Materials* 13, no. 11 (2020): 2499.

89. Y. Wu, J. Xu, Y. Liu, Y. Zeng, and G. Wu, "A Review on Anti-Tumor Mechanisms of Coumarins," *Frontiers in Oncology* 10 (2020): 592853, https://doi.org/10.3389/fonc.2020.592853.

90. M. A. Soobrattee, V. S. Neergheen, A. Luximon-Ramma, O. I. Aruoma, and T. Bahorun, "Phenolics as Potential Antioxidant Therapeutic Agents: Mechanism and Actions," *Mutation Research/Fundamental and Molecular Mechanisms of Mutagenesis* 579, no. 1 (2005): 200–213, https://doi.org/10.1016/j.mrfmmm.2005.03.023.

91. S. Shukla and S. Gupta, "Apigenin: A Promising Molecule for Cancer Prevention," *Pharmaceutical Research* 27, no. 6 (2010): 962–978, https://doi.org/10.1007/s11095-010-0089-7.

92. S. Das, J. Das, A. Paul, A. Samadder, and A. R. Khuda-Bukhsh, "Apigenin, a Bioactive Flavonoid From *Lycopodium clavatum*, Stimulates Nucleotide Excision Repair Genes to Protect Skin Keratinocytes From Ultraviolet B-Induced Reactive Oxygen Species and DNA Damage," *Journal of Acupuncture and Meridian Studies* 6, no. 5 (2013): 252–262, https://doi.org/10.1016/j.jams.2013.07.002.

93. D. Mokra, M. Joskova, and J. Mokry, "Therapeutic Effects of Green Tea Polyphenol (–)-Epigallocatechin-3-Gallate (EGCG) in Relation to Molecular Pathways Controlling Inflammation, Oxidative Stress, and Apoptosis," *International Journal of Molecular Sciences* 24, no. 1 (2023): 340.

94. E.-J. Chang, J. K. Kundu, L. Liu, J.-W. Shin, and Y.-J. Surh, "Ultraviolet B Radiation Activates NF-κB and Induces iNOS Expression in HR-1 Hairless Mouse Skin: Role of IκB Kinase-B," *Molecular Carcinogenesis* 50, no. 4 (2011): 310–317, https://doi.org/10.1002/mc.20646.

95. D. Engelberg, "The UV Response Involving the Ras Signaling Pathway and AP-1 Transcription Factors Is Conserved Between Yeast and Mammals," *Cell* 77, no. 3 (1994): 381–390, https://doi.org/10.1016/0092-8674(94)90153-8.

96. F. Guarneri, P. Custurone, V. Papaianni, and S. Gangemi, "Involvement of RAGE and Oxidative Stress in Inflammatory and Infectious Skin Diseases," *Antioxidants* 10, no. 1 (2021): 82.

97. S. J. Cooper and G. T. Bowden, "Ultraviolet B Regulation of Transcription Factor Families: Roles of Nuclear Factor-Kappa B (NF-KappaB) and Activator protein-1 (AP-1) in UVB-Induced Skin Carcinogenesis," *Current Cancer Drug Targets* 7, no. 4 (2007): 325–334, https://doi.org/10.2174/156800907780809714.

98. M. Mittal, M. R. Siddiqui, K. Tran, S. P. Reddy, and A. B. Malik, "Reactive Oxygen Species in Inflammation and Tissue Injury," *Antioxidants & Redox Signaling* 20, no. 7 (2014): 1126–1167, https://doi.org/10.1089/ars.2012.5149.

99. S. Ahmed, H. Khan, M. Aschner, H. Mirzae, E. Küpeli Akkol, and R. Capasso, "Anticancer Potential of Furanocoumarins: Mechanistic and Therapeutic Aspects," *International Journal of Molecular Sciences* 21, no. 16 (2020): 5622.

100. E. H. M. Hassanein, A. M. Sayed, O. E. Hussein, and A. M. Mahmoud, "Coumarins as Modulators of the Keap1/Nrf2/ARE Signaling Pathway," *Oxidative Medicine and Cellular Longevity* 2020, no. 1 (2020): 1675957, https://doi.org/10.1155/2020/1675957.

101. M. Sun, T. Yu, J. Zhao, et al., "Role of Flavonoids in Age-Related Macular Degeneration," *Biomedicine & Pharmacotherapy* 159 (2023): 114259, https://doi.org/10.1016/j.biopha.2023.114259.

102. H. O. A. Alharbi, M. Alshebremi, A. Y. Babiker, and A. H. Rahmani, "The Role of Quercetin, a Flavonoid in the Management of Pathogenesis Through Regulation of Oxidative Stress, Inflammation, and Biological Activities," *Biomolecules* 15, no. 1 (2025): 151.

103. I. Rahman, S. K. Biswas, and P. A. Kirkham, "Regulation of Inflammation and Redox Signaling by Dietary Polyphenols," *Biochemical Pharmacology* 72, no. 11 (2006): 1439–1452, https://doi.org/10.1016/j.bcp.2006.07.004.

104. M. Číž, A. Dvořáková, V. Skočková, and L. Kubala, "The Role of Dietary Phenolic Compounds in Epigenetic Modulation Involved in Inflammatory Processes," *Antioxidants* 9, no. 8 (2020): 691.

105. G. A. Cabral-Pacheco, I. Garza-Veloz, C. Castruita-De la Rosa, et al., "The Roles of Matrix Metalloproteinases and Their Inhibitors in Human Diseases," *International Journal of Molecular Sciences* 21, no. 24 (2020): 9739.

106. P. Brenneisen, H. Sies, and K. Scharffetter-kochanek, "Ultraviolet-B Irradiation and Matrix Metalloproteinases," *Annals of the New York Academy of Sciences* 973, no. 1 (2002): 31–43, https://doi.org/10.1111/j.1749-6632.2002.tb04602.x.

107. K. J. Gromkowska-Kępka, A. Puścion-Jakubik, R. Markiewicz-Żukowska, and K. Socha, "The Impact of Ultraviolet Radiation on Skin Photoaging—Review of In Vitro Studies," *Journal of Cosmetic Dermatology* 20, no. 11 (2021): 3427–3431, https://doi.org/10.1111/jocd.14033.

108. A. Merecz-Sadowska, P. Sitarek, E. Kucharska, et al., "Antioxidant Properties of Plant-Derived Phenolic Compounds and Their Effect on Skin Fibroblast Cells," *Antioxidants* 10, no. 5 (2021): 726.

109. Z. Zheng, L. Zhang, and X. Hou, "Potential Roles and Molecular Mechanisms of Phytochemicals Against Cancer," *Food & Function* 13, no. 18 (2022): 9208–9225, https://doi.org/10.1039/D2FO01663J.

110. L. G. Korkina, S. Pastore, E. Dellambra, et al., "New Molecular and Cellular Targets for Chemoprevention and Treatment of Skin Tumors by Plant Polyphenols: A Critical Review," *Current Medicinal Chemistry* 20, no. 7 (2013): 852–868.

111. N. K. Karamanos, A. D. Theocharis, Z. Piperigkou, et al., "A Guide to the Composition and Functions of the Extracellular Matrix," *FEBS Journal* 288, no. 24 (2021): 6850–6912, https://doi.org/10.1111/febs.15776.

112. D. M. Reilly and J. Lozano, "Skin Collagen Through the Lifestages: Importance for Skin Health and Beauty," *Plastic and Aesthetic Research* 8 (2021): 2.

113. L. Baumann, E. F. Bernstein, A. S. Weiss, et al., "Clinical Relevance of Elastin in the Structure and Function of Skin," *Aesthetic Surgery Journal Open Forum* 3, no. 3 (2021): 1–8, https://doi.org/10.1093/asjof/ojab019.

114. X. Tang, T. Yang, D. Yu, H. Xiong, and S. Zhang, "Current Insights and Future Perspectives of Ultraviolet Radiation (UV) Exposure: Friends and Foes to the Skin and Beyond the Skin," *Environment International* 185 (2024): 108535, https://doi.org/10.1016/j.envint.2024.108535.

115. H.-M. Liu, M.-Y. Cheng, M.-H. Xun, et al., "Possible Mechanisms of Oxidative Stress-Induced Skin Cellular Senescence, Inflammation, and Cancer and the Therapeutic Potential of Plant Polyphenols," *International Journal of Molecular Sciences* 24, no. 4 (2023): 3755.

116. F. Antonicelli, G. Bellon, L. Debelle, and W. Hornebeck, "Elastin-Elastases and Inflamm-Aging," *Current Topics in Developmental Biology* 79 (2007): 99–155.

117. P. Panwar, G. S. Butler, A. Jamroz, P. Azizi, C. M. Overall, and D. Brömme, "Aging-Associated Modifications of Collagen Affect Its Degradation by Matrix Metalloproteinases," *Matrix Biology* 65 (2018): 30–44, https://doi.org/10.1016/j.matbio.2017.06.004.

118. H. Lee, Y. Hong, and M. Kim, "Structural and Functional Changes and Possible Molecular Mechanisms in Aged Skin," *International Journal of Molecular Sciences* 22, no. 22 (2021): 12489.

119. D. Liang, L. Liu, Y. Zhao, et al., "Targeting Extracellular Matrix Through Phytochemicals: A Promising Approach of Multi-Step Actions on the Treatment and Prevention of Cancer," *Frontiers in Pharmacology* 14 (2023): 1186712, https://doi.org/10.3389/fphar.2023.1186712.

120. O. Gerlits, K.-Y. Ho, X. Cheng, et al., "A New Crystal Form of Human Acetylcholinesterase for Exploratory Room-Temperature Crystallography Studies," *Chemico-Biological Interactions* 309 (2019): 108698, https://doi.org/10.1016/j.cbi.2019.06.011.

121. H. Noh, S. J. Lee, H.-J. Jo, H. W. Choi, S. Hong, and K.-H. Kong, "Histidine Residues at the Copper-Binding Site in Human Tyrosinase Are Essential for Its Catalytic Activities," *Journal of Enzyme Inhibition and Medicinal Chemistry* 35, no. 1 (2020): 726–732, https://doi.org/10.1080/14756366.2020.1740691.

122. V. Nahoum, G. Roux, V. Anton, et al., "Crystal Structures of Human Pancreatic α-Amylase in Complex With Carbohydrate and Proteinaceous Inhibitors," *Biochemical Journal* 346, no. Pt 1 (2000): 201–208.

123. B. Korkmaz and F. Gauthier, "Elastase-2/Leukocyte Elastase," in *Handbook of Proteolytic Enzymes* (2013), 2653–2661.

124. A. Hartmann, J. Gostner, J. Fuchs, et al., "Inhibition of Collagenase by Mycosporine-Like Amino Acids From Marine Sources," *Planta Medica* 81, no. 10 (2015): 813–820, https://doi.org/10.1055/s-0035-1546105.

125. B. Pasternak and P. Aspenberg, "Metalloproteinases and Their Inhibitors—Diagnostic and Therapeutic Opportunities in Orthopedics," *Acta Orthopaedica* 80, no. 6 (2009): 693–703, https://doi.org/10.3109/17453670903448257.

126. K. Slinkard and V. L. Singleton, "Total Phenol Analysis: Automation and Comparison With Manual Methods," *American Journal of Enology and Viticulture* 28, no. 1 (1977): 49–55.

127. A. Emir, N. Nilofar, C. Emir, G. Coban, E. Yildiztugay, and G. Zengin, "Helianthemum Oelandicum Subsp. Incanum and Fumana Thymifolia: Characterization of LC-ESI-QTOF-MS Profiles and Their Biological Activities Based on Plant Parts and Extraction Solvents," *Kuwait Journal of Science* 52, no. 2 (2025): 100378, https://doi.org/10.1016/j.kjs.2025.100378.

128. D. M. Grochowski, S. Uysal, A. Aktumsek, et al., "In Vitro Enzyme Inhibitory Properties, Antioxidant Activities, and Phytochemical Profile of *Potentilla thuringiaca*," *Phytochemistry Letters* 20 (2017): 365–372.

129. I. Kurt-Celep, I. Nilofar, M. V. Cetiz, et al., "From Small-Scale Studies to an Encompassing View: Inhibiting Inflammation and Clinically Relevant Enzymes With Various Extracts of *Primula vulgaris* Using In Vitro and In Silico Techniques," *Food Frontiers* 6, no. 1 (2025): 329–359, https://doi.org/10.1002/fft2.473.

130. M. Yuksel Egrilmez, S. Kocturk, S. Aktan, et al., "Melatonin Prevents UVb-Induced Skin Photoaging by Inhibiting Oxidative Damage and MMP Expression Through JNK/AP-1 Signaling Pathway in Human Dermal Fibroblasts," *Life* 12, no. 7 (2022): 950.

131. İ. Kurt-Celep, A. Nihan Kilinc, M. Griffin, and D. Telci, "Nitrosylation of Tissue Transglutaminase Enhances Fibroblast Migration and Regulates MMP Activation," *Matrix Biology* 105 (2022): 1–16, https://doi.org/10.1016/j.matbio.2021.10.005.

132. L. Lescano, Z. Cziáky, İ. Kurt-Celep, et al., "Antioxidant Activity, Enzyme Inhibition, Photoprotection, Cytotoxicity, and Phytochemical Profiling of Sea Lavender (Limonium Algarvense Erben) Seed Extracts for Dermo-Cosmetic Use," *Beni-Suef University Journal of Basic and Applied Sciences* 13, no. 1 (2024): 112, https://doi.org/10.1186/s43088-024-00576-9.

133. T. H. Barak, I. Kurt-Celep, H. Dilek-Tepe, et al., "In Vitro Assessment of Dermatological Activity Potential of *Achillea clypeolata* Sm. in H2O2-Treated Human Dermal Fibroblasts," *South African Journal of Botany* 160 (2023): 1–8, https://doi.org/10.1016/j.sajb.2023.06.048.

134. M. V. Cetiz, S. Yagi, U. Kurt, et al., "Bridging HPLC-ESI-MS/MS Analysis and In Vitro Biological Activity Assay Through Molecular Docking and Network Pharmacology: The Example of European Nettle Tree (*Celtis australis* L.)," *eFood* 5, no. 6 (2024): e70026, https://doi.org/10.1002/efd2.70026.

135. E. J. Llorent-Martínez, S. Yagi, G. Zengin, et al., "Characterization of the Chemical Profiles and Biological Activities of Thesium Bertramii Azn. Extracts Using a Combination of In Vitro, In Silico, and Network Pharmacology Methods," *Fitoterapia* 180 (2025): 106329.

136. G. Zengin, M. V. Cetiz, N. Abul, et al., "Establishing a Link Between the Chemical Composition and Biological Activities of *Gladiolus italicus* Mill. From the Turkish Flora Utilizing In Vitro, In Silico and Network Pharmacological Methodologies," *Toxicology Mechanisms and Methods* 35 (2024): 1–21.

137. G. Cusumano, G. A. Flores, M. V. Cetiz, et al., "Small Steps to the Big Picture for Health-Promoting Applications Through the Use of Chickweed (*Stellaria media*): In Vitro, In Silico, and Pharmacological Network Approaches," *Food Science & Nutrition* 12 (2024): 9295–9313.

138. K. V. Dileep, K. Ihara, C. Mishima-Tsumagari, et al., "Crystal Structure of Human Acetylcholinesterase in Complex With Tacrine: Implications for Drug Discovery," *International Journal of Biological Macromolecules* 210 (2022): 172–181, https://doi.org/10.1016/j.ijbiomac.2022.05.009.

139. D. Knez, D. Diez-Iriepa, M. Chioua, et al., "8-Hydroxyquinolylnitrones as Multifunctional Ligands for the Therapy of Neurodegenerative Diseases," *Acta Pharmaceutica Sinica B* 13, no. 5 (2023): 2152–2175, https://doi.org/10.1016/j.apsb.2023.01.013.

140. A. Chiavaroli, M. L. Libero, S. C. Di Simone, et al., "Adding New Scientific Evidences on the Pharmaceutical Properties of Pelargonium Quercetorum Agnew Extracts by Using In Vitro and In Silico Approaches," *Plants* 12, no. 5 (2023): 1132, https://doi.org/10.3390/plants12051132.

141. E. Akyuz Turumtay, A. Demir, M. V. Cetiz, et al., "Metabolite Profiling of *Althaea officinalis* by HPLC-DAD-MS With In Silico and In Vitro Analysis for Therapeutic Potential," *Chemical Papers* 77, no. 10 (2023): 6235–6253.

142. M. S. Valdés-Tresanco, M. E. Valdés-Tresanco, P. A. Valiente, and E. Moreno, "gmx_MMPBSA: A New Tool to Perform End-State Free Energy Calculations With GROMACS," *Journal of Chemical Theory and Computation* 17, no. 10 (2021): 6281–6291.

143. B. R. Miller, III, T. D. McGee, Jr., J. M. Swails, N. Homeyer, H. Gohlke, and A. E. Roitberg, "MMPBSA. Py: An Efficient Program for End-State Free Energy Calculations," *Journal of Chemical Theory and Computation* 8, no. 9 (2012): 3314–3321.

144. S. Jo, T. Kim, V. G. Iyer, and W. Im, "CHARMM-GUI: A Web-Based Graphical User Interface for CHARMM," *Journal of Computational Chemistry* 29, no. 11 (2008): 1859–1865.

145. S. Yagi, G. Zengin, O. A. Eldahshan, et al., "Functional Constituents of Colchicum Lingulatum Boiss. & Spruner Subsp. Rigescens K. Perss. Extracts and Their Biological Activities With Different Perspectives," *Food Bioscience* 60 (2024): 104496.

146. J. A. Maier, C. Martinez, K. Kasavajhala, L. Wickstrom, K. E. Hauser, and C. Simmerling, "ff14SB: Improving the Accuracy of Protein Side Chain and Backbone Parameters From Ff99sb," *Journal of Chemical Theory and Computation* 11, no. 8 (2015): 3696–3713.

Supporting Information

Additional supporting information can be found online in the Supporting Information section.

Supplementary Table S1: Selected protein-ligand complexes for MM/PBSA binding free energy analysis based on molecular dynamics simulations.